AN ABSTRACT OF THE THESIS OF

Crystal M. Maddix for the degree of Master of Science in Electrical and Computer Engineering presented on March 31, 2000.

Title: Novel Phosphor Development for Alternating-Current Thin-Film Electroluminescent Devices

Abstract approved: _____

John F. Wager

The purpose of this thesis is to present an investigation of various green/red/blue alternating-current thin-film electroluminescent (ACTFEL) phosphor materials. An evaluation of YVO_4, CaS:Pb, BaS:Eu, BaS, and CaS:Sm is proffered. Additionally, lanthanide doping experiments are performed to estimate the relative hot-electron distributions in BaS, CaS, and CaSe.

Several of the materials studied show sufficient promise to warrant further investigation. The first of these is the addition of the dopant Gd to SrS:Er, which induces a significant blue shift in the normally greenish-blue electroluminescence (EL) of SrS:Er. This is a noteworthy effect since blue has traditionally been the most difficult color to obtain in ACTFEL devices. The blue-shifting action of Gd may also be useful in other ACTFEL phosphor materials. The next study of interest involves the fabrication of BaS:Eu ACTFEL devices which exhibit dim red EL. The poor EL performance is attributed to impurity or precursor incorporation; it is suggested that the use of activated deposition could result in significant improvement. Lastly, fluxing of CaS:Sm with NaF appears to enhance crystallinity in the CaS thin-film. The fluxed film exhibits EL emission at lower rapid thermal annealing (RTA) temperature of 650°C compared to the 810°C temperature normally employed. Materials studied which have poor ACTFEL characteristics include $YVO_4 : Eu$ and CaS:Pb.

A lanthanide doping study is conducted using holmium (Ho) as a luminescent impurity and BaS, CaS, and CaSe phosphor hosts. The study evalutes the relative

hot-electron distribution in a phosphor host, a parameter of interest to assess whether a host can support blue EL. The hot-electron distribution in an ACTFEL phosphor host is evaluated by the existence and intensity of high energy spectral peaks from the shielded 4f $\rightarrow$ 4f luminescent transition of Ho. It is found that BaS and CaS have electron distributions adequately heated to serve as blue EL phosphor hosts, but CaSe does not. This result correlates with the poor EL performance of blue-emitting CaSe:Cu ACTFEL devices.

Novel Phosphor Development for Alternating-Current Thin-Film Electroluminescent Devices

by

Crystal M. Maddix

A THESIS

submitted to

Oregon State University

in partial fulfillment of the

requirements for the degree of

Master of Science

Completed March 31, 2000

Commencement June 2000

Master of Science thesis of Crystal M. Maddix presented on March 31, 2000

APPROVED:

Major Professor, representing Electrical and Computer Engineering

Head of Department of Electrical and Computer Engineering

Redacted for privacy

Dean of Graduate School

I understand that my thesis will become part of the permanent collection of Oregon State University libraries. My signature below authorizes release of my thesis to any reader upon request. Redacted for privacy

Crystal M. Maddix, Author

ACKNOWLEDGEMENTS

I would like to thank Dr. Wager for all his time and effort to make this thesis publishable, and the work in it meaningful. I would like to thank everyone in the research group for their help. Specifically I'd like to thank Paul Keir, Beau Baukol and Tomoe Yokoyama for supplying ideas and the occasional reality-check.

I would also like to thank Dr. Keszler, Ben Clark, and Judith Kissick from the OSU Chemistry Department for help with both materials and theory, without which this research would not have been possible. I'd like to thank Sey-Shing Sun of Planar Systems for helping with technical issues and supplying substrates.

Finally I'd like to thank Brad Cleary, my parents Bob and Cora Maddix, and the rest of my friends and family for their patience and support.

This work was supported by the National Science Foundation under contract No. DMR-9710207.

TABLE OF CONTENTS

		Page
1	Introduction	1
2	ACTFEL Fundamentals	3
2.1	Device Operation	3
2.2	ACTFEL Device Structure	5
2.2.1	Glass Substrate	6
2.2.2	Transparent Conductor	6
2.2.3	Insulators	7
2.2.4	Phosphor Host	8
2.2.5	Luminescent Impurities	10
2.2.6	Top Conductor	11
2.3	Display Goals	12
2.3.1	CIE Coordinates	12
2.3.2	Brightness	13
2.3.3	Temperature	13
2.4	Phosphor Materials	14
2.5	Fluxing	16
3	Experimental Technique	20
3.1	Processing	20
3.1.1	Chemical Vapor Deposition	20
3.1.2	Sputtering	22
3.1.3	Evaporation	26
3.1.4	Annealing	27
3.2	Characterization Techniques	27
3.2.1	Optical Characterization	28
3.2.2	Electro-optical Characterization	29
3.2.3	Electrical Characterization	30

TABLE OF CONTENTS (CONTINUED)

		Page
4	Electroluminescent Phosphor Development	35
4.1	$YVO_4 : Eu$ as an ACTFEL phosphor	35
4.1.1	Motivation for $YVO_4 : Eu$	35
4.1.2	$YVO_4 : Eu$ Sample Preparation	36
4.1.3	$YVO_4 : Eu$ Results and Discussion	38
4.1.4	$YVO_4 : Eu$ Conclusions	41
4.1.5	$YVO_4 : Eu$ Conclusions	42
4.2	CaS:Pb as an ACTFEL phosphor	43
4.2.1	Motivation for CaS:Pb	43
4.2.2	CaS:Pb Sample Preparation	44
4.2.3	CaS:Pb Results	45
4.2.4	CaS:Pb Discussion	48
4.2.5	CaS:Pb Conclusions	50
4.3	BaS:Eu as an ACTFEL phosphor	50
4.3.1	Motivation for BaS:Eu	50
4.3.2	BaS:Eu Sample Preparation	51
4.3.3	BaS:Eu Results	52
4.3.4	BaS:Eu Discussion	54
4.3.5	BaS:Eu Conclusions	56
4.4	SrS:Er,Gd as an ACTFEL phosphor	56
4.4.1	SrS:Er,Gd Motivation	56
4.4.2	SrS:Er,Gd Sample Preparation	58
4.4.3	SrS:Er,Gd Results	59
4.4.4	SrS:Er,Gd Discussion	60
4.4.5	SrS:Er,Gd Conclusions	61
4.5	Holmium Doping Study	62
4.5.1	Motivation for Holmium Doping	62
4.5.2	Holmium Sample Preparation	63
4.5.3	Holmium Doping Results and Discussion	64
4.5.4	Holmium Doping Conclusions	66
4.6	Additional ACTFEL phosphors	66

TABLE OF CONTENTS (CONTINUED)

		Page
4.6.1	BaS ACTFEL phosphors	66
4.6.2	CaS:Sm as an ACTFEL phosphor	70
4.6.3	CaSe:Cu as an ACTFEL phosphor	71
5	Conclusions/Recommendations for Future Work	75
5.1	Conclusions	75
5.2	Recommendations for Future Work	77
Bibliography		79

LIST OF FIGURES

Figure		Page
2.1.	Energy band diagram of an ACTFEL device.	4
2.2.	Standard ACTFEL structure	5
2.3.	Inverted ACTFEL Structure	7
3.1.	Surface processes of relevance in chemical vapor deposition.	21
3.2.	RF sputtering system.	23
3.3.	Ion beam sputtering system.	25
3.4.	Sawyer-Tower test circuit.	28
3.5.	Applied voltage waveform.	30
3.6.	Typical Q-V plot of a ZnS:Mn ACTFEL device.	31
3.7.	Typical C-V plot of a ZnS:Mn ACTFEL device.	32
3.8.	Typical $Q - F_p$ plot of a ZnS:Mn ACTFEL device.	33
3.9.	Typical $Q^e_{max} - V_{max}$ plot of a ZnS:Mn ACTFEL device.	34
4.1.	Capacitance-voltage plot of a $YVO_4 : Eu$ ACTFEL device using maximum applied voltages of 180, 190, and 200 V.	37
4.2.	Charge-voltage plot of a $YVO_4 : Eu$ ACTFEL device.	39
4.3.	Q^e_{max}-V_{max} plot of a $YVO_4 : Eu$ ACTFEL device.	40
4.4.	ACTFEL device with injection layer.	42
4.5.	EL spectrum of an e-beam evaporated CaS:Pb ACTFEL device.	45
4.6.	EL spectrum of a sputtered CaS:Pb ACTFEL device.	47
4.7.	EL spectrum of a BaS:Eu ACTFEL device doped with EuS.	52
4.8.	EL spectrum of a BaS:Eu ACTFEL device doped with EuF_3.	53
4.9.	Capacitance-voltage plot of a BaS:Eu ACTFEL device using maximum applied voltages of 125, 145, 165, and 185 V.	54

LIST OF FIGURES (CONTINUED)

Figure		Page
4.10.	Capacitance-voltage plot of a BaS:Eu ACTFEL device co-evaporated with KCl using maximum applied voltages of 170, and 190 V.	55
4.11.	EL spectrum of a SrS:Gd ACTFEL device.	58
4.12.	EL spectrum of a SrS:Er ACTFEL device.	59
4.13.	EL spectrum of a SrS:Er,Gd ACTFEL device.	61
4.14.	EL spectrum of a BaS:Ho ACTFEL device.	63
4.15.	EL spectrum of a CaS:Ho ACTFEL device.	64
4.16.	EL spectrum of a CaSe:Ho ACTFEL device.	65
4.17.	EL spectrum of a BaS:Mn,KF ACTFEL device.	68
4.18.	EL spectrum of a BaS:Pb ACTFEL device.	68
4.19.	EL spectrum of a BaS:Sn ACTFEL device.	69
4.20.	EL spectrum of a BaS:Ag ACTFEL device.	69
4.21.	EL spectrum of an undoped BaS ACTFEL device.	70
4.22.	EL spectrum of a CaS:Sm ACTFEL device.	71
4.23.	Phosphor sandwich fluxing technique.	72
4.24.	EL spectrum of CaSe:Cu ACTFEL device.	73

LIST OF TABLES

Table		Page
1.	Insulators used in ACTFEL devices.	9
2.	Luminescent impurities used in ACTFEL devices.	11
3.	ACTFEL devices phosphors	15

Novel Phosphor Development for Alternating-Current Thin-Film Electroluminescent Devices

Chapter 1
Introduction

Light emission as the basis for scientific study dates back to the early Greeks who investigated naturally occurring bioluminescence from fireflies and glow-worms. V. Cascariola first discovered fluorescence, light emission caused by stimulation from an external source, in 1602 while ignoring cobbling duties to dabble in alchemy [1]. Cascariola found that light was emitted by the mineral barite after it had been exposed to sunlight; we now call this light emission mechanism photoluminescence. Hundreds of years later in 1936 Destriau found that a ZnS powder in an insulating liquid would light up when a voltage was applied to it, thus introducing the first known demonstration of high field electroluminescence [2]. Little interest in practical applications of Destriau's discovery was generated until the emergence of transparent conductors in the early 1950's. This was closely followed by the development of thin-film technology, which shifted the electroluminescence (EL) research focus from powders to thin-films [3]. The major difficulty at this point of EL development was material stability.

A major step in solving the EL reliability issue occurred in 1967 with the introduction by Russ and Kennedy of the double insulating alternating-current thin-film electroluminescent (ACTFEL) device [4]. This is the device structure most widely used today. In a double insulating ACTFEL device two insulators buffer a phosphor layer. An alternating-voltage is applied to electrodes contacted to each insulator and light is emitted when electrons are transported across the phosphor layer exciting luminescent impurities. Even with this improved structure it was not until 1974 when Inoguchi fabricated ZnS:Mn TFEL devices with good characteristics that commercial applications became viable [5], with reliability still

the foremost problem. The first commercial ACTFEL display was manufactured in 1983 by Sharp [6].

Thin-film electroluminescent (TFEL) displays constitute a small subsection of the flat panel display (FPD) genre. Other FPD technologies include liquid crystal displays (LCDs), plasma displays, and field emission devices (FEDs), with the LCD being the clearly dominant market. Compared to LCDs, TFEL displays have a wider viewing angle, better contrast ratio, better temperature response, and are more rugged. LCD's have lower power consumption, lower voltage requirements, cost less, and have full color performance.

Monochrome TFEL displays have been marketed mostly for instrumentation applications and have enjoyed success in the medical and defense markets due to their readability and ruggedness. To realize full potential in the flat panel display market the development of color displays is required. This has proven to be more difficult than expected for ACTFEL display technology. Although color ACTFEL demonstration displays were first introduced in 1993 [6], research is ongoing to develop brighter and more efficient red/green/blue ACTFEL phosphors.

This thesis will focus on the fabrication of novel ACTFEL phosphors for color displays. Chapter two introduces the ACTFEL device and reviews color ACTFEL phosphors, chapter three explains the methods used to fabricate and test ACTFEL devices, chapter four is an analysis of various novel ACTFEL phosphors, and chapter five presents conclusions and recommendations for future work.

Chapter 2
ACTFEL Fundamentals

This chapter introduces the ACTFEL device fundamentals and prevailing color ACTFEL phosphors.

2.1 Device Operation

An ACTFEL device emits light from a thin-film phosphor material which experiences a high electric field. The phosphor film, which has been intentionally doped with a luminescent impurity, is contacted through top and bottom conductors and is buffered by insulators. An AC voltage of variable frequency and maximum voltage is applied to induce a high field in the phosphor layer. Photons which are generated in the phosphor layer pass through a glass substrate to the viewer. Below a certain applied voltage, designated as turn-on, the phosphor layer and surrounding insulators simply act as three capacitors in series and no light is emitted [6, 7, 8, 9].

The physics of ACTFEL device operation above turn-on can be most clearly explained via energy band diagram analysis. Figure 2.1 illustrates the energy band diagram of an ACTFEL device above turn-on. As the applied voltage is increased above the turn-on voltage, the phosphor layer begins to conduct charge. The source of that charge is electrons trapped in interface states. As the electrical field at the interface between the phosphor and the cathodic insulator increases, electrons trapped in the most shallow interface states begin to tunnel emit. Once emitted, electrons are swept across the phosphor layer by the electric field, gaining energy along the way.

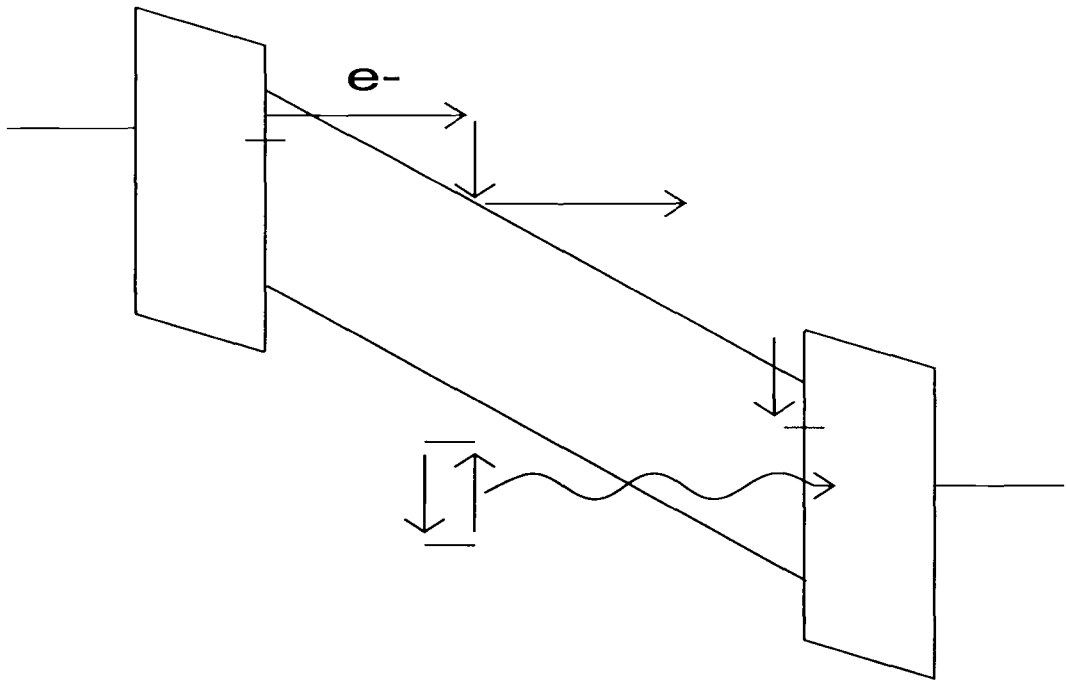

Figure 2.1. Energy band diagram of an ACTFEL device.

Occasionally, a traversing electron collides with a luminescent impurity and loses some of its kinetic energy to the impurity. The luminescent impurity becomes excited and subsequently decays back to its ground state, either emitting a photon or dissipating energy to the lattice as phonons. The transiting electron continues to transit the phosphor layer, again gaining energy until it reaches the opposite interface and is again trapped in an interface state. This cycle repeats in the opposite direction when the voltage polarity changes [7, 10, 11].

Trapped electrons at the anodic interface build up during the application of a voltage pulse. When the voltage pulse ends, this accumulation of electrons creates an electric field in the opposite direction of the previous, applied voltage-induced field. This field causes electrons in the shallowest traps to re-emit, giving rise to what is known as leakage charge. When the next voltage pulse of opposite polarity is applied, the field from electrons still trapped at the interface is now called a polarization field and is added to the applied voltage-induced field. Thus, the presence of a polarization field allows electron emission to occur at a lower

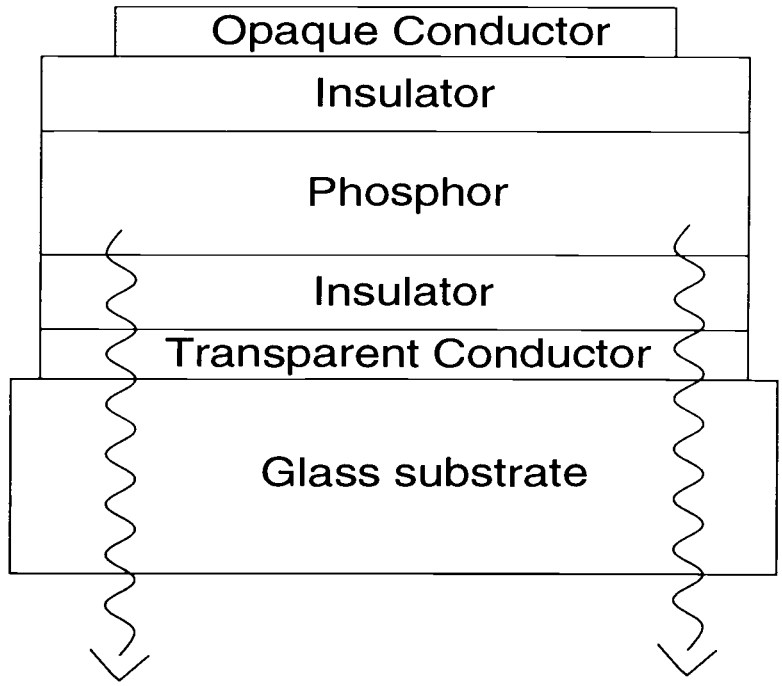

Figure 2.2. Standard ACTFEL structure

applied voltage. This succession of events occurs at a frequency of 60 Hz for normal operation and 1 kHz for standard ACTFEL testing. The performance of an ACTFEL device is typically assessed when it is driven at 40 V above the threshold voltage. Threshold voltage is defined as the voltage at which the phosphor layer begins to conduct, the threshold voltage equals the turn-on voltage when the polarization charge goes to zero.

2.2 ACTFEL Device Structure

Figure 2.2 shows a typical ACTFEL device stack consisting of; glass substrate, bottom conductor, bottom insulator, phosphor, top insulator, and top conductor. Light is generated in the phosphor layer and travels through the bottom insulator, bottom conductor, and glass substrate to the viewer. The purpose and requirements for each layer are given in the following sub-sections.

2.2.1 Glass Substrate

The typical ACTFEL structure employed has a glass substrate. An inverted stack in which the substrate is an opaque material, like silicon, and light is emitted through the top insulator and conductor, is also possible [6, 12]. Figure 2.3 shows an inverted ACTFEL stack. While an inverted structure can withstand much higher processing temperatures than the standard stack (which is limited by the temperature at which the glass substrate melts) the standard structure has two major advantages over the inverted structure.

The first advantage of the standard structure over the inverted is the ability to use an Al top conductor which enhances the self-healing breakdown properties of the top insulator. Self-healing is accomplished by creating localized open circuits around regions of poor insulation caused by pin-holes and other insulator film defects [6, 13, 14]. The inverted structure must use one of a few available transparent top conductors, none of which enhance self healing breakdown.

This leads to the second advantage of the standard ACTFEL structure over the inverted structure. In order to prevent catastrophic breakdown the top insulator in the inverted structure must have a very low defect density. Depositing a highly conformal film adds process complexity to the inverted structure that is not found in the standard ACTFEL structure.

If a standard ACTFEL structure is used, the glass substrate must transmit visible light and have as high a melting temperature as feasible. High temperature sapphire substrates, although available, are expensive. Lower temperature, lower cost glass is usually used, enhancing the need for low temperature phosphors.

2.2.2 Transparent Conductor

The emergence of the transparent conductor has made display applications feasible. It is the next layer in a standard ACTFEL structure and the top layer in an inverted ACTFEL structure. Light generated in the phosphor layer passes

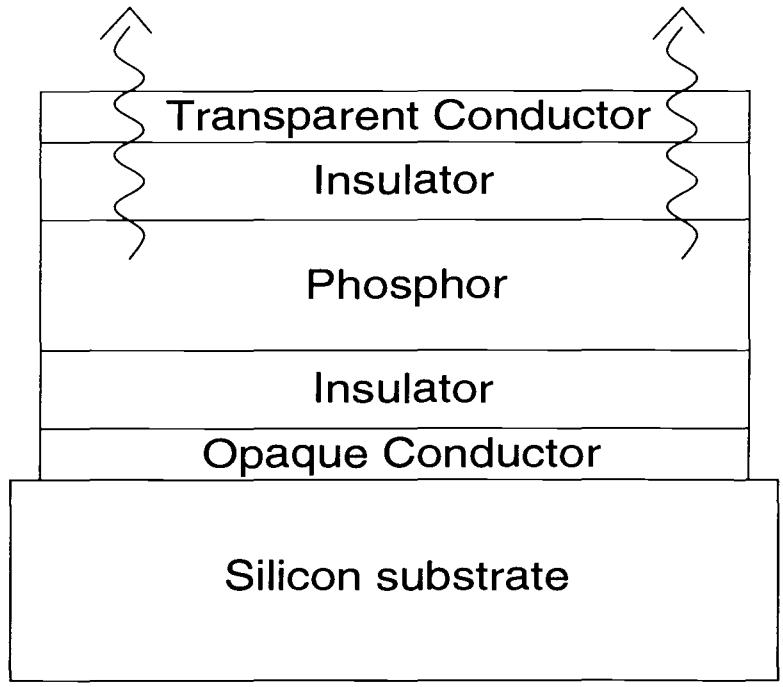

Figure 2.3. Inverted ACTFEL Structure

through this film, so it must also have high transmission in the visible region of the electromagnetic spectrum. In addition, the transparent conductor should have low resistivity to minimize power consumption. Although alternatives such as SnO_2 or ZnO:Al are available, indium tin oxide (ITO) is most commonly used. ITO is composed of 90 wt% In_2O_3 and 10 wt% SnO_2, has a resistivity of 50 ohms/sq and a direct band gap of 3.5 eV [6].

2.2.3 Insulators

The insulators in the ACTFEL structure surround the phosphor layer and provide capacitive coupling to the phosphor. Large currents, which would destroy the device, are thus prevented from passing through the phosphor layer. Desirable characteristics of the insulating layers are those which enhance this protective function of the film and have little additional affect on ACTFEL device operation.

Voltage dropped across the insulators is wasted, as far as device operation is concerned. Therefore, to minimize this wasted voltage (and power) it is desirable to maximize the capacitance of the insulating layers. The capacitance of a thin-film insulator is dependant on the dielectric constant and the thickness of the film. The capacitance is increased if the dielectric constant of the insulating layer is high and if the thickness is minimized. Note that a minimum thickness is needed in order to fulfill the insulating function of the film.

Breakdown characteristics of the insulating layers are also important. A high breakdown field is required because above turn-on, regardless of the film's capacitance, much of the applied voltage is dropped across the insulators. It is also desirable for breakdown to occur in a self-healing, as opposed to propagating, fashion. If the insulator is of the self-healing variety, a localized burn out will not destroy the device as it would in an insulator with propagating breakdown characteristics [6, 13, 14].

A final requirement for the insulator through which light is passed (the bottom insulator for a standard ACTFEL stack) is good transmission, which is not generally a limiting factor for the oxide materials used as thin-film insulators. Table 1 lists a sampling of insulators commonly used in ACTFEL processing along with some characteristics of interest, including a figure of merit defined as the relative dielectric constant multiplied by the breakdown field and deposition techniques for the films. All of the insulators listed in this table show evidence of self-healing breakdown [6].

2.2.4 Phosphor Host

The phosphor layer in the ACTFEL device consists of a host lattice intentionally doped with luminescent impurities. The purpose of the phosphor host is to provide a framework for the luminescent impurity and a medium through which the accelerating electrons pass. In order to accomplish these goals the host must conform to the following requirements; the band gap should be within the range of

Table 1. Insulators used in ACTFEL devices.

Insulator	ϵ_r	F_{BD} (MV/cm)	$\epsilon_r\epsilon_0 F_{BD}$ ($\mu C/cm^2$)	deposition method
SiON	6	6	2	CVD
Ta_2O_5	23-25	1.5-3	4-6	sputter
$BaTa_2O_6$	22	3.5	7	sputter
Y_2O_3	12	3-5	3-5	sputter/evap
Al_2O_3	8	5	4	sputter/evap
ATO	9-18	5-6.7	5.5-10	ALE

3.5-4.5 eV, the lower band gap limit is to ensure that the host does not re-absorb emitted light, the upper band gap limit of 4.5 eV is to allow for efficient electron conduction across the phosphor. In addition, the host must crystallize at a manufacturable temperature and have a fairly defect-free lattice in order to better accommodate substitutional impurities, and minimize the non-radiative decay of those luminescent impurities. Properties not inherent to the physics of ACTFEL operation, but nonetheless necessary for manufacturability, include non-toxicity and a non-hygroscopic nature [9].

ZnS is the best example of a IIb-VIb compound which acts as a good ACTFEL host lattice. Although other IIb-VIb materials have been investigated as possible ACTFEL hosts, they all have bandgaps too small to be of practical interest, with the possible exception of ZnO which has a bandgap of 3.2 eV.

IIa-VIb compounds have also received significant attention in ACTFEL material research. These compounds include SrS, CaS, and BaS, as well as the corresponding selenides. The selenides are not nearly as well explored because of their high toxicity. Members of this group are all hygroscopic to some degree and can form toxic H_2S or H_2Se upon contact with moisture. Band gaps of these ma-

terials are within the desired range of 3.5-4.5 eV (except for CaS with a bandgap of 4.8 eV and BaSe with a bandgap of 3.2 eV) [9, 15].

2.2.5 Luminescent Impurities

As the source of generated photons, the luminescent impurities are the heart of the EL process. Luminescent impurities incorporate substitutionally into a host lattice, generally at an optimal concentration of 0.1-2 wt %. For a given a phosphor host, an appropriate luminescent impurity can be selected based on efficiency, emission color, atomic radius, and ionic valence [9].

The efficiency of an impurity atom is based largely on its impact excitation cross-section. The larger the cross-section of a luminescent impurity, the higher the probability that it will be excited by an electron traversing the phosphor. No current theory appears to be able to reliably predict impact excitation cross-sections.

A luminescent impurity is also chosen based on the characteristic wavelength of light emitted. Photon emission can occur when a bound electron is excited into a higher energy level and then decays from that excited state back to its ground state. The energy difference between the two energy levels determines the wavelength of the emitted light. In some cases this energy difference can be altered by the atomic environment surrounding the luminescent impurity. The altering of energy levels due to the crystal lattice into which an atom is placed is called a crystal-field effect [15, 16]. This effect is seen strikingly in a Mn atom, a 3d transition metal, which can emit red, yellow, or green light depending on the host [15].

Some light-emitting transitions are not sensitive to crystal-field effects due to their electronic shell structure. For example, many lanthanides exhibit electroluminescence which originates from electronic transitions from one f-orbital electron state to another f-orbital electron state. The f-orbitals in the lanthanides are, to a large extent, shielded from the crystal field by outer s-, p-, and d-orbitals. There-

Table 2. Luminescent impurities used in ACTFEL devices.

Ion	Ion Valence	Radius(pm) [18]	Color	Outer Shell
Mn	2+	81	red/green/yellow	3d
Cr	4+	67	red	3d
Cu	1+	74	blue	4s
Eu	3+	131	red	4f
Ce	2+	115	blue	4f
Pb	2+	133	blue	6s
Tb	2+	106	green	4f

fore, the color of light emitted from these intra-shell transitions is not greatly influenced by the crystal field [9, 17].

Other considerations when matching impurities to hosts include size and valence matching. If the size of the luminescent impurity is very dissimilar to the size of the host cation it is replacing, it will not fit well into the lattice and lattice defects are likely to form. If the ionic valence of the lattice cation and the luminescent impurity are mismatched, vacancies are likely to be created to compensate for a charge imbalance. These vacancies will change the crystal field in the lattice and can lead to color shifting, which may or may not be desirable [19, 20].

Table 2 lists some of the most commonly used ACTFEL luminescent impurities and a few parameters of interest.

2.2.6 Top Conductor

The top layer in a standard ACTFEL structure is a second conducting film. This film should have a low resistivity (for power consumption) and be easy to deposit. It is positioned on the back side of the device so it is not necessary

for this conductor to be transparent (unless the ACTFEL device is to be fully transparent). Aluminum is the most common choice as it is inexpensive, very easy to evaporate and aids in self-healing breakdown by creating an open circuit near an insulator defect. If the ACTFEL device is an inverted structure the non-transparent conductor (the bottom conductor in this case) must be a more refractory metal, such as tungsten or molybdenum, since it must be able to withstand all subsequent high temperature processing steps without melting. Reliable opaque conductors are not difficult to find and deposit and little ongoing research is conducted on this layer of the ACTFEL device.

2.3 Display Goals

The following sub-sections specify issues of importance in the research of color phosphor materials for ACTFEL applications.

2.3.1 CIE Coordinates

In order to evaluate the chromaticity of light and show how colors relate to one another the Commission Internationale de l'Eclairage created a color map in 1931. The color map is based on an integration of the light spectrum. CIE coordinates consist of an x and y component and specify a unique position on the color map which can be achieved with a variety of different spectral combinations. A triangle created by any three points on the color map encloses all the hues which can be created by combinations of those three colors [21, 22, 23]. Therefore, such a triangle is used to determine the ideal CIE coordinates for the red, green, and blue of a full color display. The ideal CIE coordinates for full color ACTFEL displays are as follows: green (0.300, 0.600), red (0.650, 0.350), and blue (0.150, 0.100). These coordinates would put ACTFEL displays well within the range of CRT full color displays which have CIE coordinates of; green (0.312, 0.597), red (0.624, 0.337), and blue (0.157, 0.069).

2.3.2 Brightness

The human eye's response to light peaks in the green region of the electromagnetic spectrum. The eye's high sensitivity to green is followed by red then blue. Therefore, the brightness values of the RGB components in a full color display should not be equal (if they were equal the eye would interpret them as unequal). The ideal ratio of G/R/B, taken from the light response of the human eye is 6/3/1.

Very aggressive brightness goals for full color ACTFEL devices were set forth by S. Sun in 1998. These goals are based on the brightness of the dominant ACTFEL phosphor material ZnS:Mn, which has yellowish-orange emission. The brightness of a high performance ZnS:Mn ACTFEL device (at 60 Hz and 40 V above threshold) is approximately 90 fL (310 cd/m^2) [6, 9]. Therefore, a high performance green ACTFEL phosphor would have a target luminance of 90 fL (310 cd/m^2). The other corresponding target values follow as 45 fL (155 cd/m^2) for red emission and 15 fL (52 cd/m^2) for blue emission.

2.3.3 Temperature

Temperature is an important parameter in determining the manufacturability of ACTFEL displays. Since in the typical ACTFEL structure the substrate is glass, the phosphor material should not be annealed at temperatures which would cause warpage of the glass. This effectively limits the processing temperature to crystallize the phosphor host to approximately 650^{o}C. Phosphors processed above this temperature can be deposited using an inverted structure, but this creates additional reliability and manufacturing problems, as well as increased cost, as previously discussed.

2.4 Phosphor Materials

A number of materials have been investigated as possible red, green, or blue ACTFEL phosphors. The dominant ACTFEL phosphor material is ZnS:Mn, which has a yellowish-orange color with CIE coordinates of (0.500, 0.500). The ZnS:Mn spectrum is broad and peaks at 585 nm [6]. Since ZnS:Mn is the best ACTFEL phosphor known in terms of brightness, efficiency, and stability, all other potentially useful ACTFEL phosphor materials are compared to it.

The starting point for a discussion of red ACTFEL phosphor materials, and a good figure of merit to compare the performance of other materials to, is the filtered emission of ZnS:Mn. The broad peak of ZnS:Mn extends into the red portion of the electromagnetic spectrum enough to yield saturated red emission with a brightness of 70 cd/m^2 @ 60 Hz after filtering. A non-filtered material that approaches this result is SrS:Cu,Eu which gives reasonably good red emission, CIE coordinates (0.600, 0.390), and excellent brightness, 91 cd/m^2 @ 60 Hz [9]. However, the efficiency of filtered ZnS:Mn is 0.8 lm/W while it is 0.5 lm/W for SrS:Cu,Eu.

Green emission can also be obtained from the spectrum of ZnS:Mn. High brightness of 160 cd/m^2 @ 60 Hz and excellent efficiency, 1 lm/W, are obtained from a filtered green-emitting ZnS:Mn ACTFEL device. However, the color coordinates suffer in this case and the filtered emission at (0.470, 0.530) is nowhere near the optimal saturated green. Since ZnS:Mn is so bright and efficient, much work has been undertaken with ZnS and other luminescent impurities. One of the most successful green ACTFEL phosphors is ZnS:Tb which gives saturated green emission with a brightness of 90 cd/m^2 @ 60 Hz. However, after significant research the stability of this material remains a problem, casting doubt on the future of ZnS:Tb as a useful ACTFEL phosphor. Recently, a new green phosphor material, SrS:Cu,K, has been introduced and appears to hold promise since a brightness and efficiency of 52.7 cd/m^2 @ 60 Hz and 0.973 lm/W respectively, have been achieved with saturated green emission [19]. Further research into this

Table 3. ACTFEL devices phosphors

Material	CIE coordinates	Brightness (cd/m^2)	Efficiency (lm/W)	Problems
ZnS:Mn (red)	(0.65, 0.35)	70	0.8	process complexity
CaS:Eu	(0.68, 0.31)	12	0.05	refractory/ unstable
ZnS:Sm,Cl	(0.64, 0.31)	12	0.08	dim/poor efficiency
SrS:Cu,Eu	(0.60, 0.39)	91	0.5	color
SrS:Cu,K	(0.29, 0.60)	52.7	0.973	thermal quenching
ZnS:Tb	(0.30, 0.60)	90	0.6	poor stability
ZnS:Mn (green)	(0.47, 0.53)	160	1.0	color/process complexity
SrS:Cu,Ag	(0.15, 0.13)	20	0.15	unknown
SrS:Ce	(0.20, 0.38)	155	1.0	color
CaS:Pb	(0.14, 0.10)	80	?	reproducibility
(Sr0.5Ca0.5) $Ga_2S:Ce$	(0.15, 0.15)	7	0.02	dim/inefficient

material system has shown EL thermal quenching effects, defined as a decrease in luminance as the temperature is increased, currently limiting its potential for commercial applications [24]. However, early results suggest that EL thermal quenching problems may be circumvented by proper defect engineering.

The biggest challenge to full color ACTFEL displays thus far has been the lack of an adequate blue phosphor material. Therefore a substantial amount of research has been undertaken to find a blue-emitting ACTFEL phosphor with good color, brightness, and efficiency. SrS:Ce has long been a material of interest with its bright emission of 155-180 cd/m^2 @ 60 Hz and efficiency equal to that of ZnS:Mn. However, the emission color of SrS:Ce is blue-green and although somewhat bluer emission has been demonstrated, a sufficiently bright device of good blue chromaticity has yet to be demonstrated. Recent work has been published which attributes excellent characteristics to SrS:Cu,Ag namely, CIE coordinates of (0.15, 0.13) and a luminance of 20 cd/m^2 @ 60 Hz. It is currently thought that this phosphor may solve the problem of poor blue ACTFEL emission [25, 26, 27]

Table 3 lists some of the more successful RGB ACTFEL phosphor materials [6]. As each performance improvement is made to red, green, or blue materials, research efforts must intensify to achieve corresponding improvements to the other two colors. Although large advances have been recently made, many more breakthroughs are needed to make full color ACTFEL display technology competitive in the display market.

2.5 Fluxing

A flux agent is introduced into a compound to alter physical properties of the material. Traditionally fluxing has been used in sintered powders to increase densification by changing the interface energy, increasing grain boundary mobility, increasing the vacancy concentration, or increasing diffusion rates [28, 29]. Fluxing is a technique which adds many experimental options to the optimization of ACTFEL phosphor materials. Fluxing can be used in a variety of ways to

improve phosphor performance: as a crystallinity enhancer, charge compensator, or co-activator.

Crystallinity in a thin-film can be improved with the addition of a flux agent. For ACTFEL phosphor thin-film applications, a crystallized lattice is desirable because; it improves carrier transport, allows light to be more efficiently out-coupled, and enhances luminescent impurity incorporation into the lattice. Effective flux ions diffuse readily into a host lattice, creating vacancies. The presence of vacancies (especially cation vacancies) allows luminescent impurities to more easily diffuse into the lattice. The flux agent then assists in recrystallization, again by increasing the diffusivity of ions that are to be incorporated into the lattice. The resulting fluxed thin-film should have a well-distributed impurity concentration and be well-crystallized.

Engineering the vacancy concentration in an ACTFEL phosphor film with charge compensators is another important flux application [30]. Luminescent impurities generally substitutionally replace a cation in a host lattice. If the impurity and cation do not have the same valence, a vacancy may be created in the lattice in order to maintain charge balance.

For example, in SrS:Ce, Ce^{3+} ions substitutionally replace Sr^{2+} ions in the lattice, yielding donors. This creates a charge imbalance which may correct itself by forming strontium vacancies (i.e. acceptors) in the lattice [31]. Such a process in which compensating vacancies form as a consequence of acceptor or donor doping is denoted self-compensation [32, 33, 34]. Note that in the SrS:Ce system self-compensation can be circumvented by K^{1+} co-doping; a K^{1+} ion sitting on a Sr^{2+} site constitutes an acceptor; if an equal number of K^{1+} acceptors and Ce^{3+} donors are incorporated into the lattice, charge neutrality is achieved via donor-acceptor compensation instead of by vacancy self-compensation.

Ideally donor/acceptor compensation is achieved by introducing equal concentrations of luminescent impurity and charge compensator into the film. In reality, the fluxing nature of the charge compensating ions allows them to readily

diffuse in the film so that they often end up at grain boundaries or in clusters. Therefore, the flux concentration initially introduced is usually larger than the luminescent impurity concentration.

Altering the vacancy concentration in a phosphor film by adding charge compensating flux agents can also result in a shift in the emission spectrum of the luminescent impurity. Work by Li and Keszler illustrates this principal in SrS:Cu powders [35]. Their work shows that adding Na flux to SrS:Cu powders shifts the photoluminescent (PL) spectrum from blue to green. They conclude that added fluxes with a +1 valence act as acceptors and initiate the creation of compensating sulfur vacancies. The observed PL color shift from blue to green is due to a pairing of Cu^{1+} ions (acting as acceptors on a Sr^{2+} site) and S vacancies (acting as donors). The Cu ion in the $Cu - V_s$ pair experiences a weaker crystal field than a 6-coordinated Cu, and therefore undergoes a red-shift.

Li and Keszler's work was extended to SrS:Cu ACTFEL devices by Keir *et al.* [19]. In this work, a blue SrS:Cu,F ACTFEL device with a chromaticity of CIE coordinates (0.164, 0.268) is shifted to green with the addition of alkaline metal fluorides, the most effective being KF producing a shift to coordinates (0.289, 0.596). The same $Cu - V_S$ pair theory is used to explain Keir's thin-film results. Green Cu emission from a SrS:Cu,K ACTFEL device originates at a Cu^{1+}-V_S complex. KF fluxing of the SrS:Cu film increases the number of sulfur vacancies, resulting in more $Cu - V_S$ complexes, and thereby shifting the spectrum to green.

Another example of color-shifting using flux dopants is given in the work of Velthaus *et al.* which investigates SrS:Ce [31]. In this case, Ag is fluxed into the ACTFEL device to blue-shift the greenish-blue emission of SrS:Ce. Ag^{1+} sitting on a Sr^{2+} site acts as an acceptor, charge compensating for the Ce^{3+} impurity ion which also sits on a Sr^{2+} site and acts as a donor. This extrinsic compensation results in bluer SrS:Ce ACTFEL devices than normally observed.

Fluxes are also sometimes used in ACTFEL devices to achieve luminescent energy-transfer. Energy-transfer refers to a down-conversion process in which a

high energy photon emitted from one luminescent impurity is used to excite a second luminescent impurity. This type of interaction occurs in CaS:Eu,Ce ACT-FEL devices; when a Ce^{3+} impurity is impact excited and subsequently decays back to it's ground state, it emits a high energy photon which is then absorbed by a Eu^{2+} impurity which decays, resulting in red luminance.

Chapter 3
Experimental Technique

This chapter introduces some of the techniques used in fabricating and characterizing ACTFEL devices.

3.1 Processing

This section is devoted to a brief discussion of processing technologies used in the fabrication of novel ACTFEL phosphors. This section is not meant to be comprehensive; a more thorough treatment of various processing methods can be found in the "Silicon Processing for the VLSI era" series by Wolf and Tauber [36].

3.1.1 Chemical Vapor Deposition

Chemical vapor deposition (CVD) is often used to deposit insulators and ACTFEL phosphor materials. The primary steps of a CVD process are as follows: The CVD chamber is initially evacuated to a base pressure. The evacuated chamber is subsequently backfilled with process gases necessary for the desired reaction. Reactant and inert process gases are usually introduced into the CVD reactor at a flow rate established by a mass flow controller (MFC). The reactant gases in the chamber diffuse to the substrate. The gas molecules then migrate along the surface, and chemically react with one another to form a film. Byproducts from the chemical reaction and excess gas molecules desorb from the surface and are pumped out of the chamber. Thermal energy for the reaction at the surface of the substrate is supplied by a substrate heater.

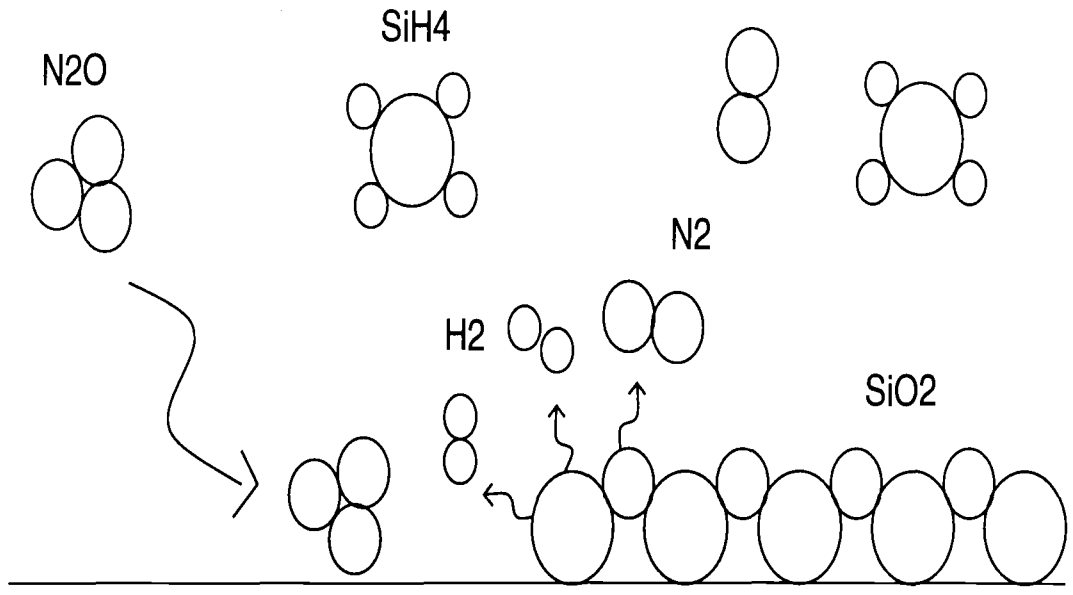

Figure 3.1. Surface processes of relevance in chemical vapor deposition.

An example of a typical CVD process is shown in Fig. 3.1 which illustrates the deposition of Silicon dioxide (SiO_2) by the following reaction:

$$SiH_4 + 2N_2O \rightarrow SiO_2 + 2N_2 + 2H_2 \tag{3.1}$$

One type of CVD process is plasma enhanced chemical vapor deposition (PECVD). PECVD utilizes a plasma to supply energy, in addition to thermal energy from a substrate heater, to enhance the chemical reaction rate at the surface of the growing film. A plasma, or more precisely a glow discharge, consists of a mixture of neutral gas molecules, ions, free radicals, and electrons. Electrons, energized by an electric field, collide with gas molecules and; impact excite (causing light emission), impact ionize, or elastically deflect from larger atomic, molecular, or ionic species [37]. In this way, energy is coupled to the molecules and ions which react at the surface of the substrate.

In the case of PECVD, the gas reactants are components of the glow discharge and as such arrive at the substrate with sufficient energy to react and form a film. PECVD can be performed at much lower substrate temperatures than traditional

CVD, making it attractive for processing which would be adversely affected by a high temperature.

Another type of CVD process is denoted atomic layer epitaxy (ALE). ALE has been used to create high quality phosphor, insulator, and conductor thin-films for ACTFEL device applications [38, 39]. ALE thin-films tend to be highly conformal and to have a low defect density which is especially important in insulator films to enhance the reliability of the ACTFEL device. An ALE run consists of an alternating introduction of two or more gas species into the chamber. Each introduced species tends to react only with dissimilar atomic species present on the surface of the substrate and not with itself. In this way a single atomic layer of the reactant species is deposited on the substrate surface. The first gas is purged from the system and a second reactant species, which reacts with the newly deposited layer (but again, not with itself) is introduced. The result is an atomic layer of the desired compound. It is not difficult to see how this process results in highly defect-free films. One of the drawbacks of ALE deposition is a long development time to determine appropriate precursor gases. Another negative aspect is the slow deposition rate since at least two system purges must occur for each atomic layer of a compound.

3.1.2 Sputtering

One of the most common thin-film deposition techniques, sputtering, is often used in ACTFEL processing because of its inherent ability to deposit compounds with good stoichiometry. This is a necessary trait for phosphor films which consist of both a host compound and a luminescent impurity. The sputtering process begins with generation of a glow discharge as a source of high energy ions. The glow discharge is initiated by introducing a gas between two electrodes and applying a voltage to the electrodes. The energetic ions are directed at a target composed of the material to be deposited. Target atoms are dislodged by the bombarding ions and transport away from the target in all directions including toward the sub-

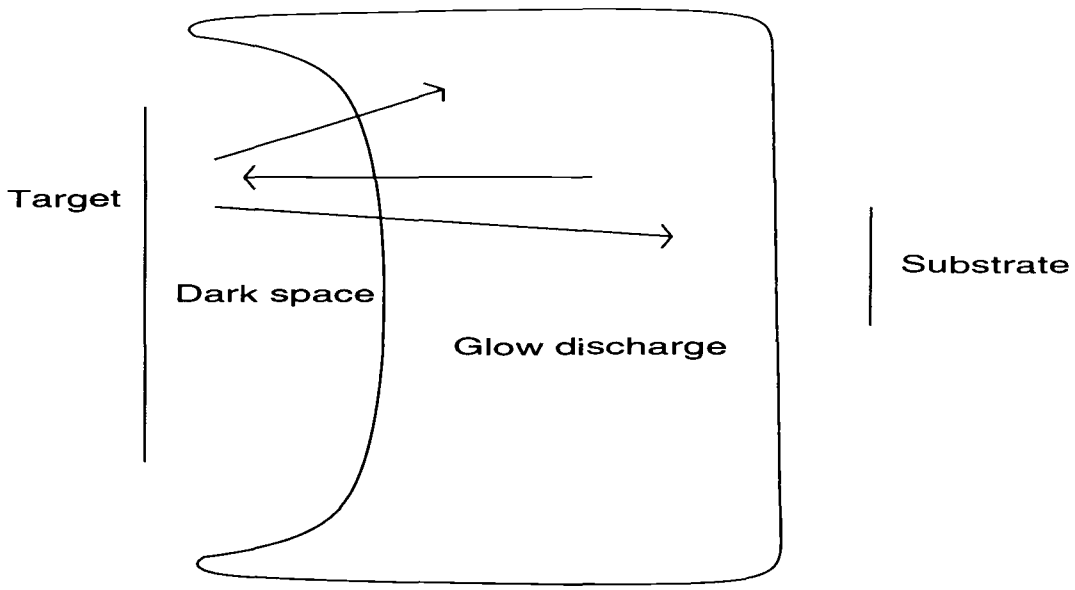

Figure 3.2. RF sputtering system.

strate. The substrate is heated so that arriving atoms migrate to lattice positions and form a film. The area just in front of the target is known as the dark space. Most of the voltage applied to the electrodes is dropped across the dark space. Positive ions in the glow discharge are attracted to a negatively charged cathode and electrons are repelled. Since electrons are lighter, and therefore move faster, there is a net accumulation of positively charged ions in front of the cathode which enhances the electric field. This area is dark because the enhanced electric field accelerates electrons rapidly, so much so that if they collide with an atom they cause impact ionization instead of excitation. The target is placed at the cathode and the substrate at the anode. This brief summary of the sputtering process describes a direct current (DC) sputtering system. DC sputtering, however, is ineffective as a deposition technique for insulators. Since three of the five layers in an ACTFEL device are insulators, an alternative sputtering method is required.

The source of the difficulty in sputtering insulators is related to the self-sustaining nature of the glow discharge. When ions from the glow discharge hit the target surface, they often cause the emission of secondary electrons in addition

to target atoms. These secondary electrons enter the dark space and are rapidly accelerated toward the anode, providing a source of electrons to sustain the glow discharge. If the target being sputtered is an insulator, once secondary electrons are removed they cannot be replaced and a positive charge builds up on the target surface. Eventually the positive charge building up at the cathode brings it close enough in potential to the anode that the glow discharge is extinguished.

Insulating targets can be sputtered with a radio frequency (RF) voltage source. RF sputtering employs an alternating polarity voltage source so that electrons move back and forth between the two electrodes and do not need to be supplied by the target. The minimum required voltage frequency is determined by the time it takes to build up positive charge at the negative electrode and extinguish the glow discharge, which is 1-10μs. 13.56 MHz has been federally designated as a frequency for RF sputtering systems to prevent interference with other radio signals. A self-bias is generated by the build up of negative charge on the target surface, again the result of electrons traveling faster than heavier ions. This self-bias directly in front of the target aids in the acceleration of ions to sputtering velocities.

Another way to make up for the lack of secondary electrons in insulating targets, and thereby open up sputter deposition as an ACTFEL fabrication process, is to add electrons from an external source. Ion beam sputtering creates and sustains a glow discharge using an electron emitting filament. Ions are extracted from the glow discharge and accelerated toward a target. The accelerating ions then sputter the target in the usual way [40, 41, 42]. An illustration of an ion-beam sputtering system is shown in Fig. 3.3. Ion beam sputtering allows a pressure differential to exist between the glow discharge chamber and the target chamber. Deposition can therefore occur at lower pressures than DC or RF sputtering which means fewer contaminants and faster deposition rates. Positive charge from the bombarding ions typically builds up on the surface of an insulating target, necessitating a second electron emitter to neutralize the target.

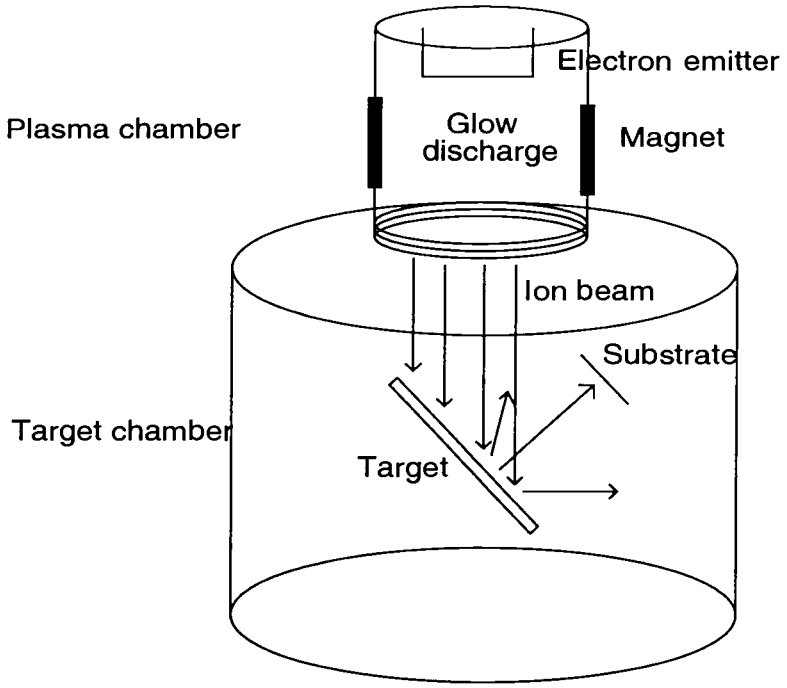

Figure 3.3. Ion beam sputtering system.

Sputtering is often used in phosphor processing because of its fitness to deposit compounds. Since atoms are physically removed with an excess of energy from the target, differences in chemical properties of molecules do not preclude them from being simultaneously sputtered. Ideally, the sputtering system self-compensates for different material sputtering rates since as any one atom is preferentially removed from the target surface its concentration is reduced, making removal of the other target components more likely. This process is not necessarily sufficiently self-compensating to retain target stoichiometry in the film, but initial target stoichiometry can be adjusted to compensate. The many control parameters in a sputtering process mean that thickness and thin-film properties can be easily adjusted. Disadvantages of sputtering include high cost, slow deposition rate, the necessity of target preparation which in some cases can be a lengthy effort, and the requirement of a relatively high pressure in the chamber to sustain the glow discharge which can result in film contamination.

3.1.3 Evaporation

Many types of conducting and insulating thin-films potentially useful in ACT-FEL device fabrication can be evaporated. Additionally, a significant fraction of phosphor materials can be evaporated thus offering a wide range of device fabrication possibilities. Evaporation is an expeditious thin-film processing technique and, as such, is ideally suited for a research environment (and is commonly used in manufacturing as well). Evaporation can be accomplished by heating a material to its vaporization temperature with either a current or an electron beam.

Material to be thermally evaporation is placed in a boat, usually tungsten since it is highly refractory and unlikely to cause contamination. The boat is heated by passing a current through it, which causes the material in the boat to vaporize. Alternatively, the material can be placed in a crucible made of any number of materials including alumina or carbon, which is held by a wire or boat and evaporated in the same manner. The vaporized material deposits onto a substrate, the temperature of which can be elevated. Evaporation occurs in high vacuum so contamination from background gases is minimized. Simple thermal evaporation is limited by two factors; the melting point of the boat and the conductor holding the boat, and the thermal conductivity of the material and its surroundings.

An alternative to thermal evaporation is electron beam (e-beam) evaporation which utilizes an e-beam to heat the material to be deposited. Again, the material is vaporized and deposited onto a substrate. In the case of e-beam evaporation, only the top surface of the source material is heated, so contamination from the crucible is minimized. E-beam evaporation can be employed to deposit more refractory materials than thermal evaporation since it is able to heat the material efficiently and in a localized manner. It is also easier to deposit compounds since an e-beam tends to give the material sufficient energy to evaporate more congruently. E-beam systems do not have the simplicity of a thermal evaporator and in order to evaporate the powder form of a material it must be pressed and sintered into dense pellets.

Evaporation has a speed advantage over other deposition techniques since very little preparatory work is needed for materials (with the exception of e-beam pellet formation) and the actual process time can be very fast. However, highly refractory materials cannot be evaporated, uniformity is typically poor, and it is difficult to control evaporation rates and therefore composition. In a manufacturing environment, run-to-run consistency is low compared to sputtering or CVD.

3.1.4 Annealing

A processing step common to many deposition techniques is a post-deposition anneal. The as-deposited thin-film is usually not well crystallized and an annealing cycle is required for crystallization. There is a great deal of evidence that the brightness and efficiency of ACTFEL devices is increased with an increased polycrystalline grain size [43, 44, 45, 46, 47]. An effective method for post-deposition annealing is via rapid thermal annealing (RTA). An RTA cycle quickly reaches the desired temperature and stays there for only a short time, which allows the glass substrates used in ACTFEL devices to withstand a higher temperature than can be applied, without warpage, in a traditional furnace anneal. Furnace annealing is not without a place in ACTFEL processing; materials may form better crystal lattices if annealed for multiple hours in a furnace and high volume manufacturing is most efficiently accomplished via furnace annealing.

3.2 Characterization Techniques

Once fabricated, ACTFEL device operation must be evaluated. ACTFEL device operation is often assessed using the test circuit shown in Fig. 3.4 (normally called the Sawyer-Tower arrangement) [48]. The test circuit consists of an arbitrary waveform generator which produces a trapezoidal waveform used to stimulate the device, shown in Fig. 3.5, a high voltage amplifier, a resistor used

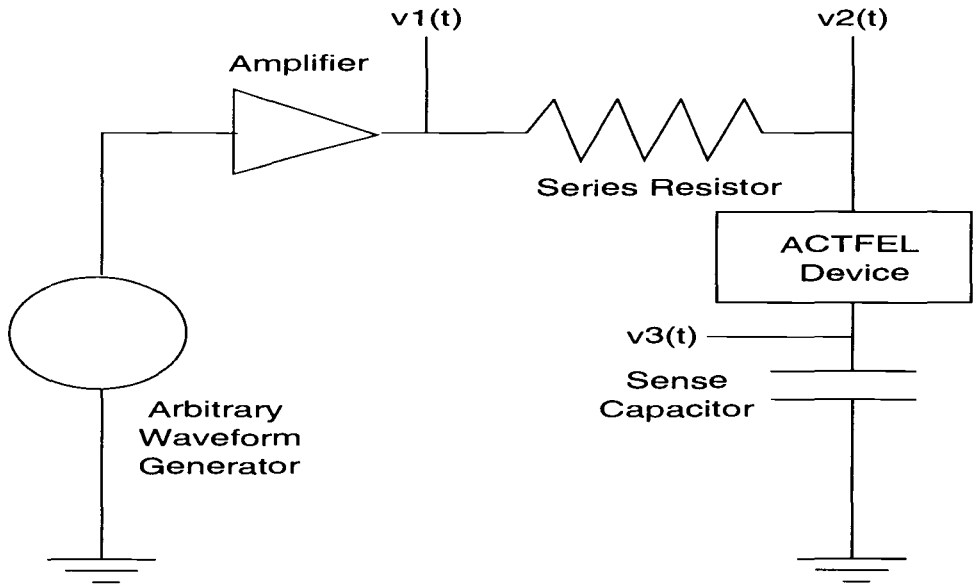

Figure 3.4. Sawyer-Tower test circuit.

to limit current to the device, and a sense capacitor. Device operating parameters can be determined optically, electro-optically, and electrically. Optical data is obtained from the face of the device with external light sources minimized. Raw data for electrical characterization is gathered at v_1, v_2, and v_3 as indicated in Fig. 3.4. The most common techniques to characterize ACTFEL devices are briefly summarized in the following section [49].

3.2.1 Optical Characterization

Optical characterization of an ACTFEL device is accomplished by measuring its spectrum and brightness. A light spectrum measures the relative luminance versus wavelength of light emitted. Data is generally limited to the visible and near UV/IR wavelengths. The spectrum is used to determine the chromaticity of light emission as well information about which energy states are transitioning (by comparing known energy levels of the given luminescent impurity). The chromaticity is evaluated as a set of x and y CIE coordinates.

A brightness measurement gives the amount of light emitted normal to the surface of the device, per unit surface area of the device and is given in units of Candela per square meter (cd/m^2) or Ft. Lambert (fL). Brightness in an ACTFEL device is voltage and frequency-dependent [9]. Data is typically taken at a frequency of 60 Hz and a voltage of 40 V over threshold, and therefore called L_{40}, to aid in comparison of results between researchers. Brightness is also dependent on the shape of the applied voltage waveform; unfortunately there is little consensus on this parameter in reported results. Both spectral and brightness results reported in this work are measured using a Photo Research 650 spectrophotometer.

3.2.2 Electro-optical Characterization

Electro-optical characterization involves measurement of an optical output as a function of an electrical input. Brightness-voltage and efficiency-voltage are common electro-optical measurements [8].

Brightness-voltage (B-V) characterization, also called luminance-voltage (L-V), is performed by recording the steady state luminance in the device, as a function of the applied voltage. The B-V curve typically shows an initial steep rise in luminance at threshold. The luminance slope decreases shortly after threshold and transitions to a constant slope with increasing applied voltage.

Efficiency, η, is calculated by dividing luminance by power input.

$$\eta = \pi \frac{L}{P} \text{ (lm/W)} \tag{3.2}$$

The π factor accounts for light output at viewable angles other than normal to the surface (which is what the B-V measurement obtains). Power density is computed from the input current and voltage [8, 50]. A typical efficiency curve shows a decrease in efficiency with an increase in voltage just above threshold. This decrease in η reflects the decrease in slope of the B-V curve just above threshold.

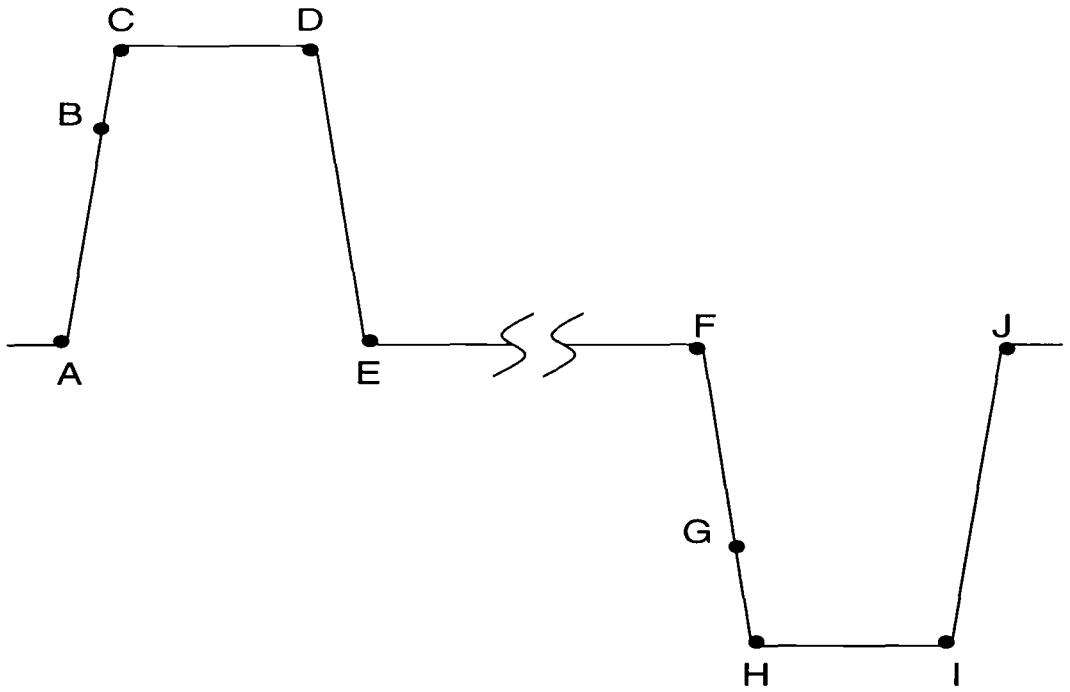

Figure 3.5. Applied voltage waveform.

The efficiency also decreases with the frequency of the driving waveform since, although luminance increases, power input must increase faster with frequency.

3.2.3 Electrical Characterization

Electrical characterization can take many forms, the most common being charge vs. voltage (Q-V), capacitance vs. voltage (C-V), charge vs. phosphor field ($Q - F_p$), and maximum external charge vs. maximum voltage (Q^e_{max}-V_{max}) plots [49].

An external charge versus instantaneous voltage plot (i.e. a Q-V plot) shown in Fig. 3.6, is taken using one applied voltage waveform [8, 51, 52]. Steady state is first established in the device. The Q-V plot is then traced in a counter-clockwise direction. The letters on the plot correspond to points on the applied voltage waveform in Fig. 3.5. Point A represents the beginning of the positive voltage pulse. The charge measured at point A is a polarization charge left at the

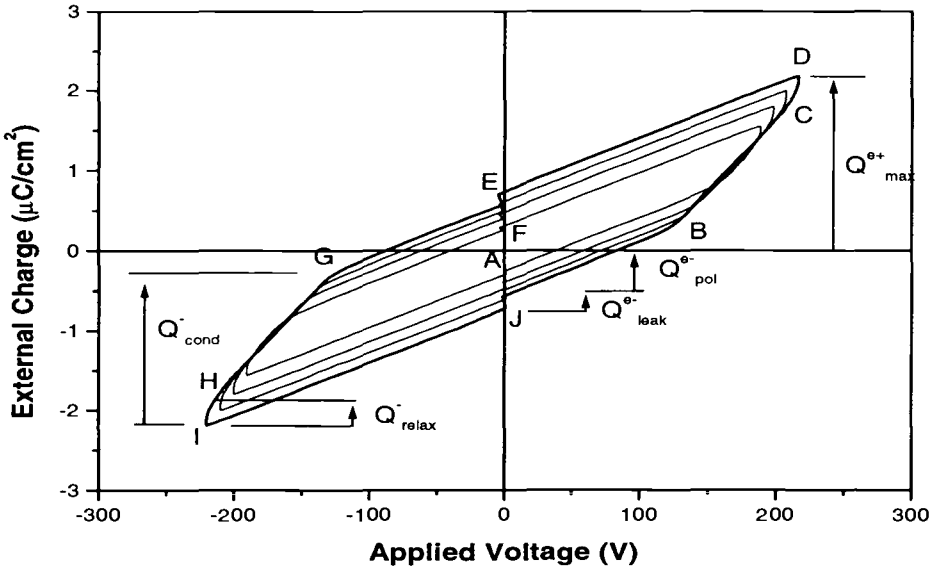

Figure 3.6. Typical Q-V plot of a ZnS:Mn ACTFEL device.

phosphor/insulator interface from the previous pulse of opposite polarity. The rising edge of the voltage pulse spans points A-C, with point B the voltage at which the device reaches turn-on (V_{to}). The applied voltage is held constant from points C-D; since electrons continue to move across the phosphor the internal electric field decreases. The charge transfered while the electric field is diminishing is termed relaxation charge. Charge transported across the phosphor during the active portion of device operation is conduction charge and is measured between points B and D. The applied voltage decreases from points D to E, and the applied voltage remains at zero from points E to F. Leakage charge emitted between points E and F reduces the polarization charge built up for the next voltage pulse of opposite polarity. The remaining curve is traced during the negative voltage pulse and is analogous to the positive half just reviewed.

Capacitance-voltage (C-V) data is obtained from a derivation of the Q-V curve. Although the data is not new, the presentation makes certain aspects of the device's behavior easier to see. Fig. 3.7 shows a typical C-V curve. The

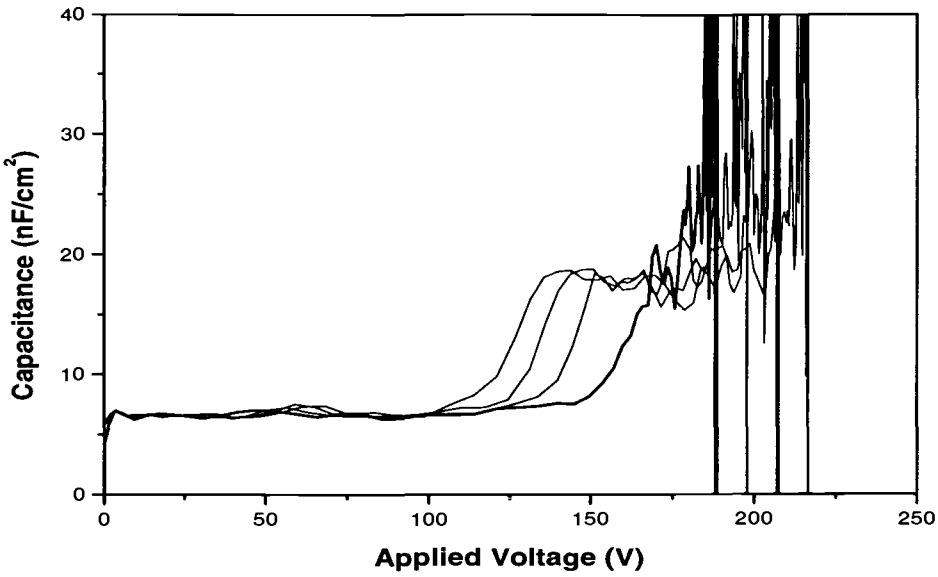

Figure 3.7. Typical C-V plot of a ZnS:Mn ACTFEL device.

capacitance before V_{to} is a series combination of the capacitance of the thin-film insulators and the phosphor layer. Above V_{to}, when the phosphor layer begins to conduct, the capacitance will ideally be the series combination of just the two insulators. A C-V graph is rarely ideal, however, and the non-idealities yield additional information about the device [51, 53, 54, 55]. A measured capacitance greater than that calculated from expected physical dielectric constants and thicknesses of the constituent thin-films indicates the existence of space charge in the device [56, 57]. If the measured capacitance is smaller than that calculated the phosphor layer is not completely shunted and the conduction current is limited. The shape of the C-V curve near V_{to} also gives information about whether electrons are being sourced from the bulk, or primarily from interface states.

The internal charge versus phosphor field ($Q - F_p$) curve constitutes another manipulation of the Q-V data. A $Q - F_p$ plot is traced clockwise and the lettering and charges correspond to those of the Q-V curve. The data has been transformed in a $Q - F_p$ graph to reflect all charges as internal charges for direct comparison

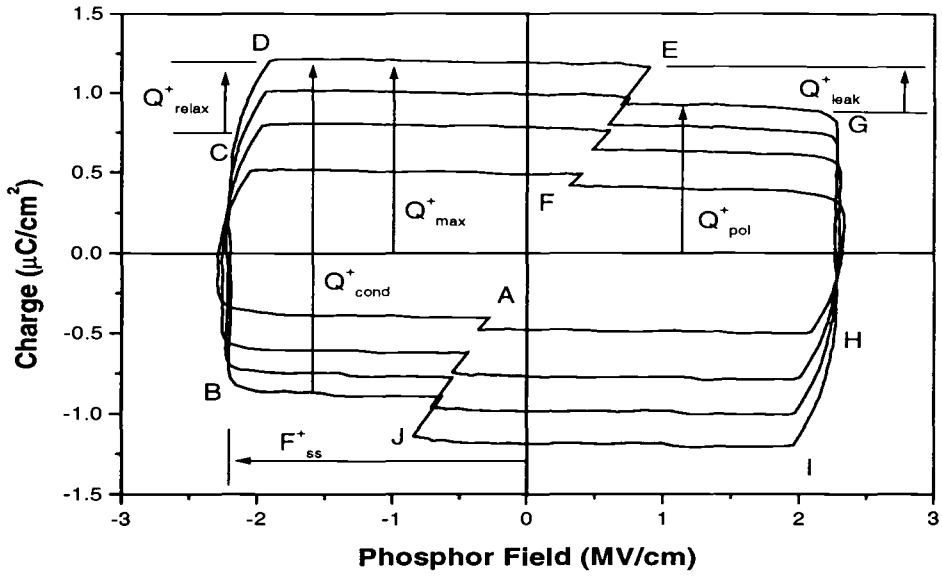

Figure 3.8. Typical $Q - F_p$ plot of a ZnS:Mn ACTFEL device.

with one another [58, 59]. In addition the comparison of charge to phosphor field instead of applied voltage clarifies some of the ACTFEL device physics. The phosphor field is calculated from the applied voltage and material parameters of the thin-films.

A typical external transferred charge-maximum applied voltage ($Q^e_{max}-V_{max}$) plot from a ZnS:Mn ACTFEL device is shown in Fig. 3.9. This plot is generated by recording the maximum external charge for each applied voltage pulse (evaluated at the top right corner in the Q-V plot of Fig. 3.6 for the positive pulse). As the applied voltage is ramped, the maximum external charge at each voltage constitutes the $Q^e_{max} - V_{max}$ curve. The two important aspects of this curve are: the inflection point, and the slope of the curve.

The inflection point where the curve changes slope, can be interpreted as the threshold voltage of the device since it is the point where charge begins to move across the phosphor. The slope of the curve above threshold indicates how efficiently charge is transferred across the phosphor. If the slope is less than the

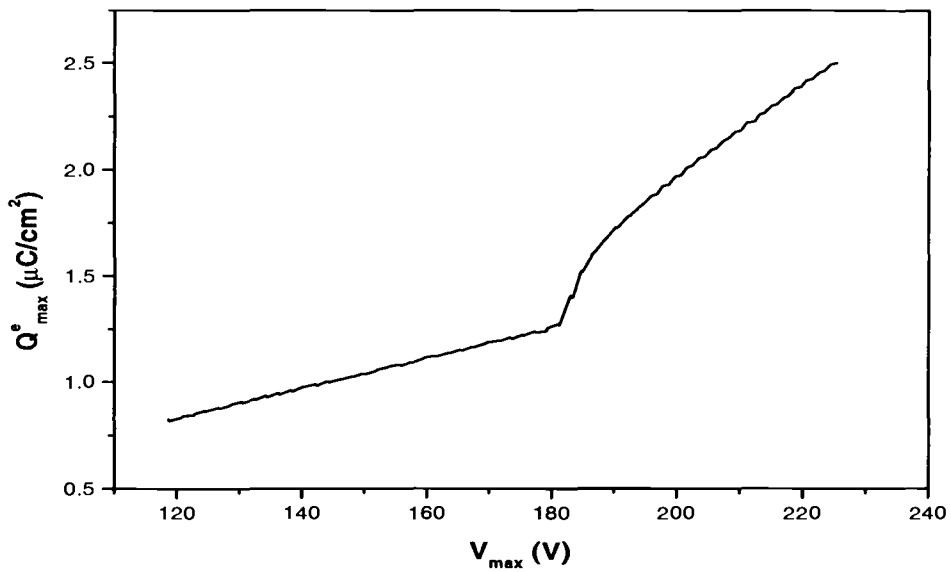

Figure 3.9. Typical $Q^e_{max} - V_{max}$ plot of a ZnS:Mn ACTFEL device.

insulator capacitance (slope $< C_i$), the phosphor layer is not fully shunted, indicating poor charge transfer. If the slope is greater than the insulator capacitance (slope $> C_i$), some form of carrier multiplication and trapping is occurring, indicating the formation of space charge. If the slope equals the insulator capacitance (slope $= C_i$), the phosphor layer is conducting and no space charge is being created; this situation occurs for sufficiently large overvoltages (e.g. at 200V in Fig. 3.9).

Chapter 4
Electroluminescent Phosphor Development

This chapter introduces and evaluates ACTFEL devices fabricated with novel ACTFEL phosphor materials.

4.1 $YVO_4 : Eu$ as an ACTFEL phosphor

4.1.1 Motivation for $YVO_4 : Eu$

Oxides are not traditionally considered appropriate ACTFEL phosphor materials because of their typically large band gaps. This assumption has been recently challenged by the emergence of a number of bright EL devices fabricated with oxide materials. Zinc germinate doped with manganese ($ZnGeO_4 : Mn$) gives bright green emission, as does zinc silicate also doped with manganese ($ZnSiO_4 : Mn$) [60]. Minami summarizes a few of these EL oxide phosphors and reports spectra and brightness values [61].

Yttrium oxide-based phosphors have been used extensively as cathodoluminescent phosphors. Yttrium vanadate doped with europium ($YVO_4 : Eu$) was reported in 1964 by Levine and Palilla [62] who introduced it as a red-emitting cathodoluminescent phosphor for color television. They found the material to have a dominant spectral peak at 612 nm and CIE coordinates of (0.670, 0.330), using a material doped with 5% Eu (they found little difference from 3-10%). YVO_4 as the preferred host for the Eu^{3+} ion was superseded four years later by yttrium oxysulfide (Y_2O_2S) investigated by Royce *et al.* [63]. Yttrium tungstate ($Y_2(WO_4)_3$) doped with Eu^{3+} was presented by Kano *et al.* [64] much later. Both

of these materials gave successively brighter emission with identical spectral characteristics. More recently, Tseng *et al.* [65] initiated another study on $Y_2O_2S : Eu$ as a pressed powder film and reported cathodoluminescence and photoluminescence with emission lines at 616 and 626 nm.

All of these Eu-doped phosphors luminesce near the characteristic 612 nm line emission of Eu^{3+}. This 612 nm emission characteristic is relatively independent of the phosphor host because Eu^{3+} luminescence arises from a shielded 4f $\rightarrow$ 4f transition. Specifically, the 612 nm emission arises from a $^5D_0 \rightarrow {}^7F_2$ transition, an electric-dipole emission that is allowed when there is no inversion symmetry in the surrounding lattice [15, 17].

Their use in cathodoluminescent (CL) applications, coupled with recent encouraging ACTFEL oxide phosphor results, suggests that yttrium oxide compounds should be further investigated as ACTFEL phosphor materials. An investigation into yttrium oxide-based ACTFEL devices has been undertaken by Sowa *et al.* [66]. This study evaluates a $Y_2O_2S : Eu$ device with a ZnS injection layer, producing a hot-carrier injection type ACTFEL device. Dim red emission of 2 cd/m^2 was obtained at a driving frequency of 10 kHz. No reports have been found of attempts to fabricate ACTFEL devices using $YVO_4 : Eu$ despite this materials excellent brightness and chromaticity in both cathodoluminescent and photoluminescent applications. In order to evaluate the possibility of a red-emitting EL phosphor from this material, the following study is performed.

4.1.2 $YVO_4 : Eu$ Sample Preparation

$YVO_4 : Eu$ devices are fabricated with the standard ACTFEL device structure of Fig. 2.2. A thin-film of the transparent conductor ITO is sputter deposited onto a glass substrate. Following this a bottom insulator of aluminum titanium oxide (ATO) is deposited by ALE. These two layers are deposited at Planar Systems. The $YVO_4 : Eu$ film is RF sputtered from one of two targets which contain either 1% or 2.5% Eu_2O_3.

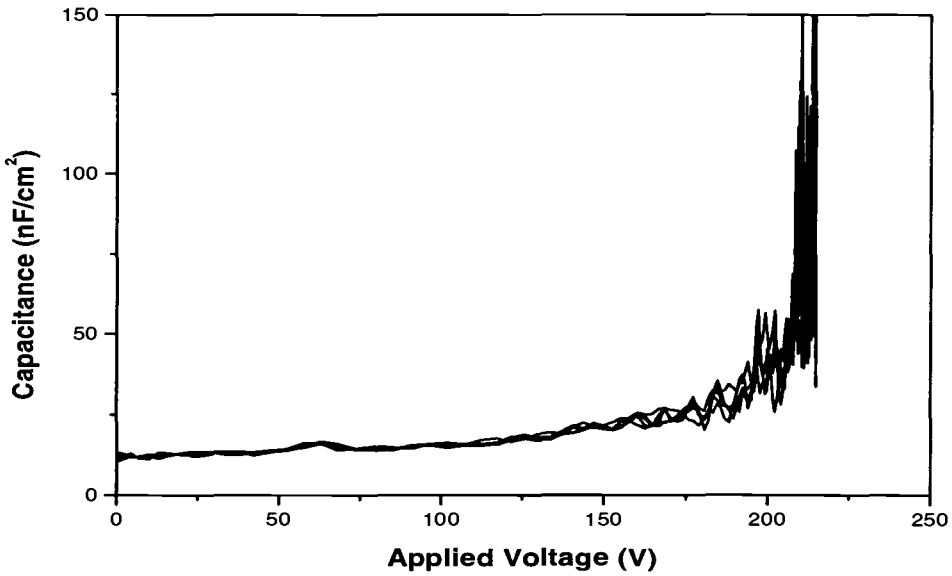

Figure 4.1. Capacitance-voltage plot of a YVO_4 : Eu ACTFEL device using maximum applied voltages of 180, 190, and 200 V.

The target material was prepared and cold-pressed by Judith Kissick of the OSU Chemistry Department. The YVO_4 : Eu material was formed from stoichiometric amounts of Y_2O_3, NH_4VO_3, and Eu_2O_3 powders fired together at 1000°C for 2-3 hours. The target was then pressed and sintered at 1200°C for 48 hours. The target is sputtered in a mixture of 80% argon and 20% oxygen with a background pressure of 30 mT. Material is deposited at a rate of 2 nm/min to a thickness of 200-300 nm while the substrate is slowly passed in front of the target to improve film quality. After phosphor deposition, the device is RTAed for 2 minutes at 750°C in an oxygen ambient. A top insulator of SiON is deposited via PECVD with a thickness of 200 nm, and a top conductor of aluminum is thermally evaporated to an approximate thickness of 200 nm.

4.1.3 $YVO_4 : Eu$ Results and Discussion

Excellent photoluminescence is observed for all $YVO_4 : Eu$ samples fabricated. PL is visible as deposited, and is bright red after annealing. However, despite the encouraging PL, no electroluminescence is observed for any $YVO_4 : Eu$ ACTFEL device tested. Initial electrical characterization of $YVO_4 : Eu$ ACTFEL devices shows evidence of low-field conduction. This trend can be most easily seen in the C-V curve of Fig. 4.1. As mentioned in Section 3.2.3, a rise in the measured capacitance indicates that the phosphor layer is beginning to conduct charge. Comparison of a C-V curve from a ZnS:Mn ACTFEL device (Fig. 3.7) to Fig. 4.1 indicates that the phosphor layer of the ACTFEL device shown in Fig. 4.1 begins to conduct at a comparatively small applied voltage, and has a very gradual slope. Charge that traverses the phosphor under low field conditions is not able to gain enough energy from the applied electric field to impact excite luminescent impurities, and is therefore useless from an ACTFEL operation standpoint.

Low field conduction can occur if electrons are present in shallow traps in the phosphor or at the phosphor/insulator interface. Shallow traps coupled with a yellow-tinge to the film suggests that the YVO_4 layer may be non-stoichiometric. A vanadium deficiency was postulated as the source of the non-stoichiometry. In an effort to correct this, a thin-film of vanadium oxide (V_2O_5) was deposited on top of the sputtered device before the annealing step and fluxed into the YVO_4 film. The V_2O_3 flux was found to suppress some of the very low-field conduction characteristics, but did not result in visible EL.

A typical Q-V plot for a $YVO_4 : Eu$ device is shown in Fig. 4.2. Compare this curve to the typical Q-V curve for a ZnS:Mn ACTFEL device shown in Fig. 3.6. Conspicuously missing in Fig. 4.2 is point B, the turn-on voltage, where the phosphor layer begins to conduct an appreciable amount of charge. Instead, the Q-V curve is constant throughout the rising edge portion of the applied voltage waveform.

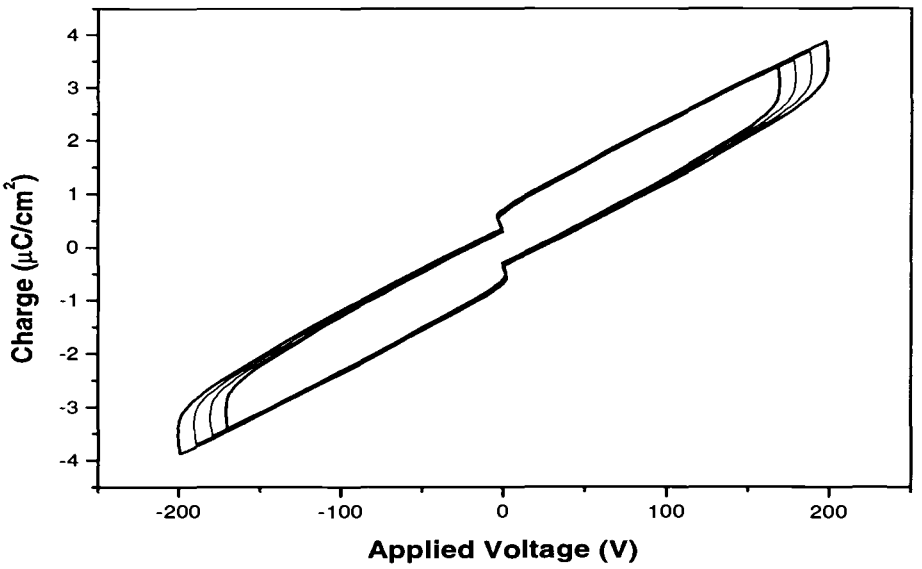

Figure 4.2. Charge-voltage plot of a $YVO_4 : Eu$ ACTFEL device.

The apparently lazy conduction in the $YVO_4 : Eu$ ACTFEL devices studied corresponds to a device operating by bulk charge injection. In an interface injection ACTFEL device, like ZnS:Mn, as the field increases a point is reached at which a significant number of carriers can be emitted from interface states into the phosphor bulk. In a ZnS-type ACTFEL device there are far fewer bulk traps than interface traps and the bulk traps that exist are scattered throughout the phosphor layer [57, 67]. Carriers sourced from bulk traps are emitted at varying applied voltages, depending on the local field, and do not traverse the entire phosphor thickness, decreasing the kinetic energy of the electron and the probability of luminescent impurity impact excitation. Therefore, the lack of an abrupt turn-on voltage in $YVO_4 : Eu$ ACTFEL devices suggests bulk-sourced charge from relatively shallow trap states. It should be noted that the maximum fields present in the phosphor layer of the $YVO_4 : Eu$ ACTFEL devices are easily as high as 5 MV/cm, and would be sufficient to emit electrons from all but very deep interface states if they existed.

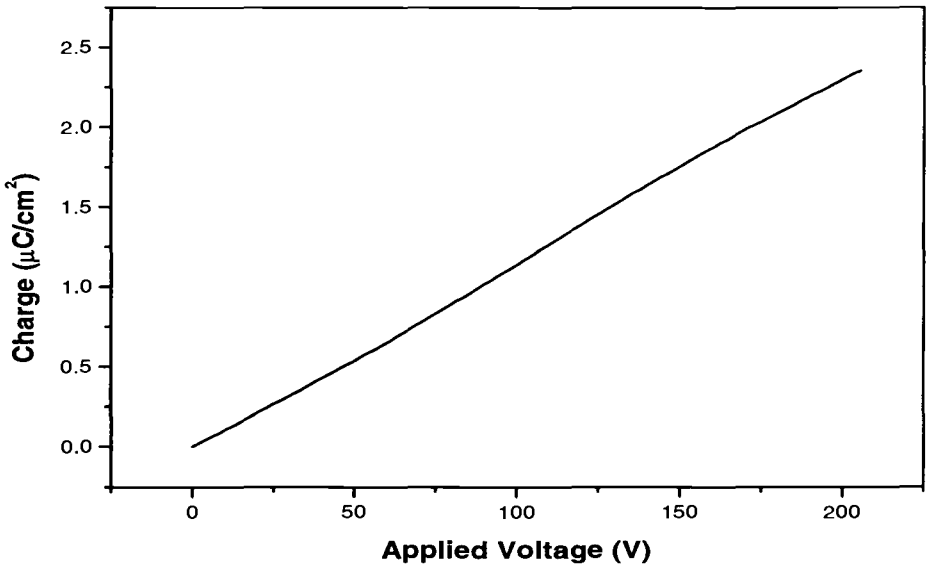

Figure 4.3. Q^e_{max}-V_{max} plot of a $YVO_4 : Eu$ ACTFEL device.

Note that all of the Q-V curves shown in Fig. 4.2 are hysteretic, so it is apparent that some conduction current does flow across the phosphor. The nearly vertical jump in the Q-V curves near the maximum applied voltage indicates that most of the current is due to relaxation charge, meaning that this charge flows when the applied voltage is at its constant, maximum value. The transfer of charge at the maximal applied voltage causes the phosphor field to relax.

Another indication that these $YVO_4 : Eu$ ACTFEL devices source charge mainly from the phosphor bulk instead of from interface states, is the fact that the polarization charge is constant as seen in the Q-V curve of Fig. 4.2. Polarization charge arises from the build up of conduction electrons trapped at interface states [49, 52]. As the maximum applied voltage to the $YVO_4 : Eu$ device increases, there is a limit to the number of interface states available to be filled and thus a constant amount of polarization charge.

Compare this plot to Fig. 3.9 which is a typical $Q^e_{max} - V_{max}$ curve for a ZnS:Mn ACTFEL device. The constant slope seen in the $YVO_4 : Eu$ $Q^e_{max} - V_{max}$

plot (Fig. 4.3) clearly indicates non-abrupt charge transfer. In fact, the constant slope of the $Q^e_{max} - V_{max}$ curve indicates that transferred charge capacitance is constant, which means that the YVO_4 never conducts sufficiently to shunt the phosphor layer.

Additional evidence that EL performance, or lack thereof, of $YVO_4 : Eu$ ACTFEL devices appears to be related to transport, not luminescent impurity properties is given from attempts to co-dope $YVO_4 : Eu$ with alternative luminescent impurities such as Er, Ho, or Mn. ACTFEL devices co-doped in this manner have all failed to produce any visible luminescence. These impurities are added to the $YVO_4 : Eu$ film by flux doping as follows. After sputter deposition of $YVO_4 : Eu$, a thin layer of the desired impurity is thermally evaporated onto the sample. The impurity ions diffuse into the YVO_4 host lattice during a 750°C RTA. The lack of EL from the co-doped $YVO_4 : Eu$ ACTFEL devices, coupled with the observed bright PL of the phosphor film indicates that it is the electrical characteristics, more specifically poor electron injection and transport, and not some aspect of the luminescent impurity which is the root of the poor EL performance.

No visible EL was observed from any of the sputter deposited $YVO_4 : Eu$ ACTFEL devices fabricated in this study. The low-field conduction observed in these devices may be due to non-stoichiometry or crystal defects, and as such could probably be eliminated with further process optimization. It seems unlikely, considering the non-abrupt turn-on characteristics that may indicate a charge injection deficiency, that a traditional injection-type ACTFEL device will be viable. However, the lack of an abrupt turn-on represents a serious obstacle to using $YVO_4 : Eu$ as an ACTFEL phosphor material.

4.1.4 $YVO_4 : Eu$ Conclusions

If a lack of interface states is the EL-limiting factor in $YVO_4 : Eu$ devices, it should be possible to fabricate injection-type ACTFEL devices. Injection-type

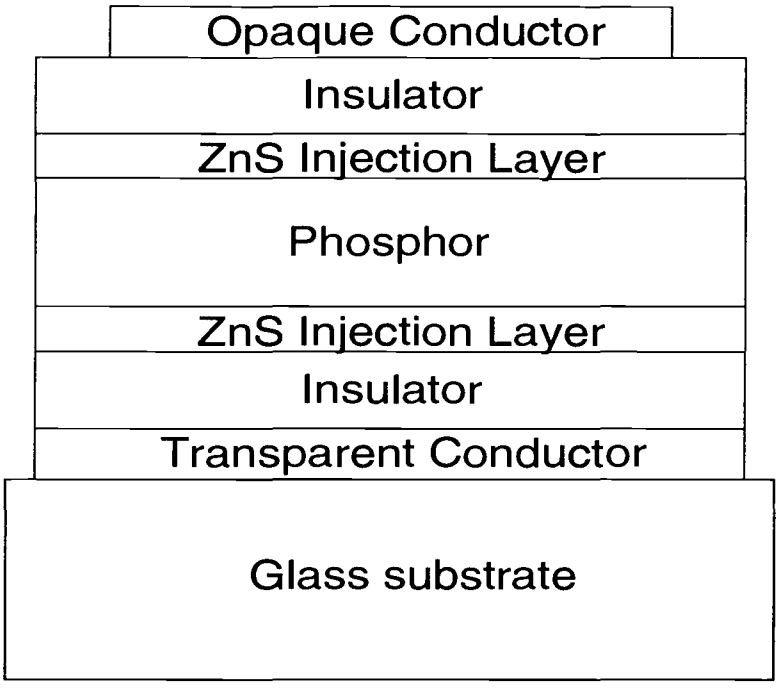

Figure 4.4. ACTFEL device with injection layer.

devices, shown in Fig. 4.4, consist of a doped phosphor that is buffered by undoped ZnS layers used to inject charge into the device. As mentioned earlier, a device of this type was successfully fabricated with $Y_2O_2 : Eu$ [66]. However, issues of matching threshold voltage and maximum phosphor field limit the brightness of these devices.

4.1.5 $YVO_4 : Eu$ Conclusions

A novel ACTFEL device which utilizes bright PL emission and could therefore induce luminescence from a $YVO_4 : Eu$ thin-film is discussed by Young-Jae Cho *et al.* [68]. The thin-film stack starts with a UV-emitting EL phosphor. A second phosphor thin-film which exhibits bright PL is deposited over the UV emitting layer. The PL of the top phosphor layer is excited by the EL of the lower phosphor layer. $YVO_4 : Eu$ is highly suited for this sort of device since its PL emission is strong. Cho's study includes $YVO_4 : Eu$ excited by UV EL emission from a

$GdCl_3$ thin-film, and reports a luminance of 50 cd/m^2 @ 5 kHz. Studies of this alternative ACTFEL device may prove fruitful but it is likely that the overall efficiency will be low since two luminescent processes are necessary for visible emission.

4.2 CaS:Pb as an ACTFEL phosphor

4.2.1 Motivation for CaS:Pb

Lead (Pb), used as a luminescent impurity, is known to emit in the UV to blue region of the electromagnetic spectrum [15]. Both SrS and CaS have been of some interest as host materials for lead-based luminescent materials. Luminescence of Pb as a luminescent impurity in SrS, SrSe, CaS, and CaSe powders was extensively studied by Yamashita *et al.* in the late 70's and early 80's [69, 70]. Their work treated the question of emission from monomer or dimer centers. A monomer is a single Pb ion substitutionally incorporated into the lattice, while a dimer is a complex of two Pb ions near one another in the lattice. Yamashita's work concluded that UV emission results from Pb monomers and visible blue emission originated at Pb dimers. Initial work on CaS:Pb as an electroluminescent material was presented by Nykanen *et al.* [71] in 1992. ALE devices were fabricated with 4-6% Pb which resulted in 450 nm blue emission, but the luminescence was a low 2.5 cd/m^2 @ 300 Hz. Poelman *et al.* [72] later fabricated CaS:Pb ACTFEL devices using an electron beam technique; again a very weak blue EL was obtained this time with a broad spectrum. The latest and most remarkable paper on CaS:Pb was presented by S. Yun *et al.* who reported blue EL at 440-460 nm with CIE coordinates (0.14, 0.10) and a brightness of 80 cd/m^2 @ 60 Hz [73]. However, efficiency values were not reported and it has since become clear that these spectacular brightness values were obtained at an extremely high power, as the ACTFEL insulators were found to be leaky. In order to explore the viability of this phosphor system, a study of CaS:Pb was undertaken.

4.2.2 CaS:Pb Sample Preparation

CaS thin-films are e-beam evaporated, CaS e-beam pellets are produced by Ben Clark of the OSU Chemistry Department. CaS is formed by firing calcium oxide in a H_2S environment for 2 hours at 1200°C. The calcium sulfide powder is then cold-pressed into pellets and sintered up to 1400°C.

CaS:Pb ACTFEL devices are fabricated using the standard ACTFEL device structure shown in Fig. 2.2. To deposit the phosphor film, a CaS pellet is e-beam evaporated while a lead compound is thermally co-evaporated from an alumina crucible. The concentration of lead in the sample is established by the evaporation rates of the CaS and Pb sources. The glass substrate, pre-coated with an ITO transparent conducting layer and an ATO insulating layer, is held at a temperature of 300°C during evaporation. After phosphor deposition the film is RTAed at 810°C for 2 1/2 minutes in an argon ambient. A silicon oxynitride insulator is PECVD deposited on top of the phosphor with a substrate temperature of 350°C. Finally, an Al patterned top conductor is thermally evaporated onto the sample.

Flux doping studies of e-beam evaporated CaS:Pb thin-films are conducted using the half sample technique [9]. After phosphor deposition, one half of a 1" x 1" glass substrate is covered and a thin-film of a fluxing compound is thermally evaporated onto the uncovered half. When the sample is annealed, the flux diffuses down into the phosphor film. In this manner, a comparison of fluxed and unfluxed devices on the same substrate can be made, minimizing the amount of process variation between ACTFEL devices.

A similar study of flux doping of sputtered CaS:Pb thin-films was undertaken in conjunction with S. Sun of Planar Systems. CaS:Pb samples are sputtered by S. Sun at Planar Systems, from a target of CaS doped with PbS, and a GaS flux agent. The target was prepared by Jim Kane of the Sarnoff Research Center, Princeton N.J. The flux doping study performed at OSU on sputtered samples also utilizes the half sample fluxing technique.

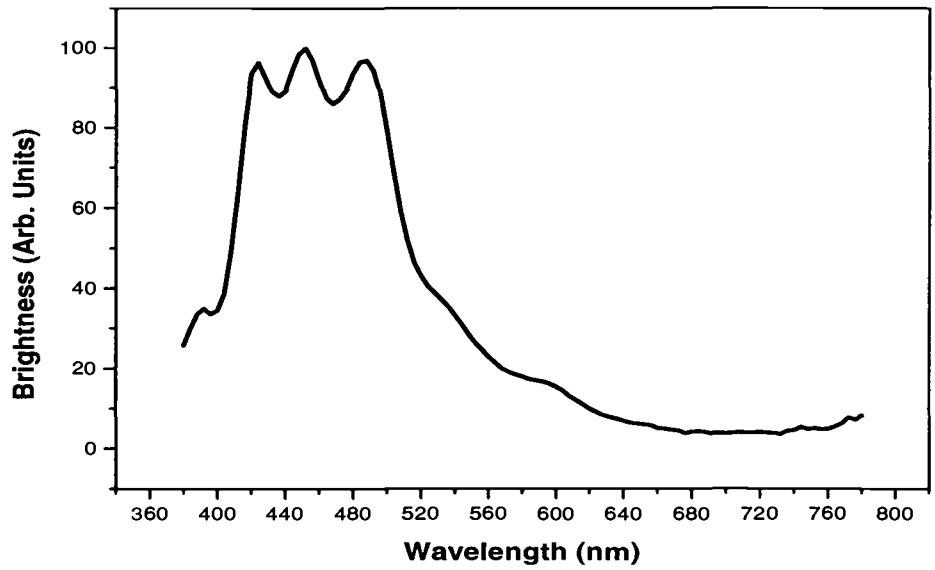

Figure 4.5. EL spectrum of an e-beam evaporated CaS:Pb ACTFEL device.

4.2.3 CaS:Pb Results

Optimization of emission from e-beam evaporated CaS:Pb ACTFEL devices is accomplished by first undertaking a study of lead sources. ACTFEL devices containing PbS, $PbCl_2$, and PbF_2 dopants are compared. The brightest emission is seen from devices fabricated using a lead chloride ($PbCl_2$) source. Therefore, $PbCl_2$ is the lead source used for all in-house CaS:Pb samples subsequently fabricated in this study.

The emission spectrum from an e-beam evaporated CaS:Pb ACTFEL device is shown in Fig. 4.5. This spectrum shows a broad blue emission with three dominant spectral peaks at 420, 450, and 485 nm. The CIE coordinates for this sample are (0.193, 0.204). The middle peak at 450 nm in this evaporated CaS:Pb spectrum compares to the emission from most other published data on CaS:Pb [71, 73]. The possible origin of the side peaks at 420 and 485 nm is discussed in Section 4.2.4.

The next level of optimization of CaS:Pb ACTFEL devices relates to the lead concentration in the phosphor film. Lead dimers have been suggested to be responsible for blue emission [69, 70], and Nykanen *et al.* report maximum brightness at high lead concentrations of 4-6 %, while Poelman *et al.* and Yun *et al.* argue respectively that large Pb concentrations are harmful because of; clustering, which leads to green-red emission, or crystallinity disruption [71, 72, 73]. It is likely that an unusually large impurity concentration would be desirable if it could be reliably incorporated to maximize dimer formation. A concentration study based on the ratio of evaporated $PbCl_3$ to CaS from 1% to 6% was performed. The need for a fairly large Pb concentration is confirmed by the maximum L_{40} brightness of 1.29 cd/m^2 @ 1 kHz obtained from a sample fabricated with an evaporation ratio of 3% $PbCl_3$. Note that the actual Pb concentration in the film is probably somewhat less than 3% since the substrate is heated.

The final area of optimization attempted with e-beam evaporated CaS:Pb ACTFEL devices concerns the addition of flux dopants into the CaS:Pb thin-film. Co-evaporation of potassium chloride (KCl) or sodium chloride (NaCl) during phosphor deposition has a positive effect on the ACTFEL device brightness, increasing the L_{40} brightness from 1.29 cd/m^2 @ 1 kHz to 3.24 cd/m^2 @ 1 kHz. Flux layer doping of KCl or NaCl also increases the brightness, but it is less effective than flux dopant incorporation via co-evaporation, resulting in a maximum L_{40} brightness of 2.3 cd/m^2 @ 1 kHz. Sputtered CaS:Pb ACTFEL devices fabricated by Planar Systems have EL emission from a dominant peak at 420 nm, as shown in Fig 4.6. The measured luminance from sputtered CaS:Pb ACTFEL devices of 3-4 cd/m^2 @ 1 kHz is comparable to the luminance of 1 cd/m^2 @ 1 kHz obtained from unfluxed e-beam deposited CaS:Pb ACTFEL devices. The spectral character and chromaticity of the sputtered films are slightly different than the violet emission of e-beam evaporated samples as seen in Fig 4.5. The single dominant emission peak at 420 nm from sputtered CaS:Pb films is at a slightly shorter wavelength than previously reported CaS:Pb emission [71, 73].

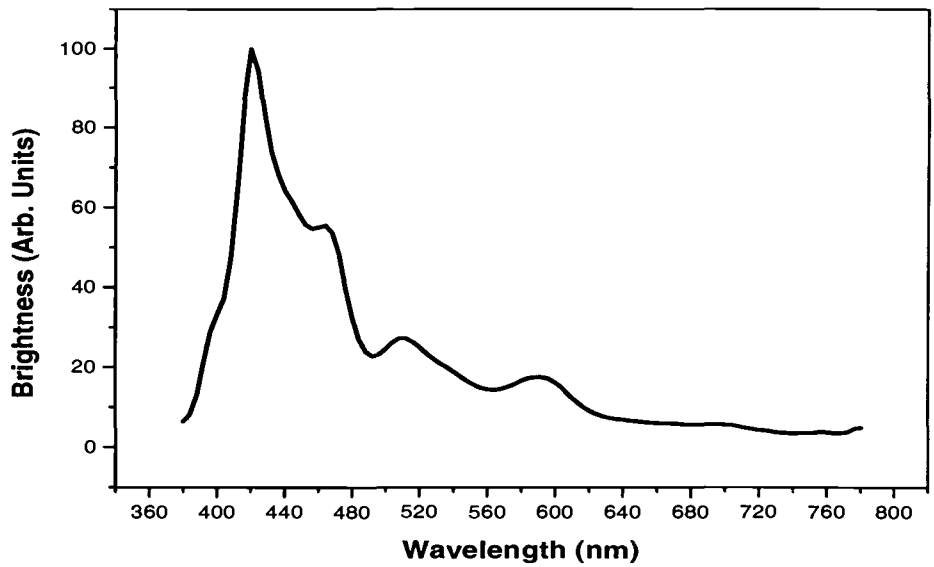

Figure 4.6. EL spectrum of a sputtered CaS:Pb ACTFEL device.

In an attempt to increase brightness and compare sputtered CaS:Pb samples to e-beam deposited CaS:Pb samples, several sputtered films are subjected to a flux doping study. Since the sputtered CaS:Pb films had already been deposited, flux doping via co-evaporation was not possible. Thus, this study was conducted using the half sample flux layer doping technique. An increase in the L_{40} brightness from 2.52 cd/m^2 @ 1 kHz to 4.80 cd/m^2 @ 1 kHz is observed for a sputtered CaS:Pb sample flux doped with a KCl layer. This increase in brightness is similar to that observed for e-beam deposited samples flux doped with KCl. Flux layer doping using NaCl did not improve the brightness of sputtered CaS:Pb films. The brightest sputtered CaS:Pb ACTFEL device measured is 4.99 cd/m^2 @ 1 kHz, using KCl flux layer doping.

4.2.4 CaS:Pb Discussion

The origin of the side peaks at 420 and 485 nm in the e-beam evaporated CaS:Pb samples shown in Fig. 4.5 is not clear. It may be a result of non-uniformity of the crystal field with the side peaks due to Pb monomers, dimers, or clusters in a variety of lattice configurations. If this is the case the number of side peaks should increase with increasing lead concentrations, and the resultant increase of irregular Pb formations. In support of this theory Poelman *et al.* suggest that the green-red EL emission that they observe as the Pb concentration is increased is due to the formation of Pb clusters [72]. However, emission at high Pb concentrations is weak and therefore additional spectral peaks are not observed. It is likely that the Pb distribution in sputtered CaS:Pb films is more consistent than that of e-beam deposited films due to the nature of the sputtering process, which is very effective at randomizing the distributing of target atoms in a depositing thin-film. In the case of evaporated samples, Pb is co-evaporated with the CaS thin-film, making the formation of Pb clusters more likely. A better distribution of Pb ions in the CaS lattice will produce fewer variations in emission and hence the side peaks should be, and are, greatly reduced in the sputtered CaS:Pb ACTFEL device shown in Fig. 4.6.

The decrease in brightness seen in CaS:Pb ACTFEL devices fabricated at evaporation ratios of $PbCl_2$/CaS greater than 3% is probably due to concentration quenching [74]. Concentration quenching occurs at high luminescent impurity concentrations where rapid resonant transfer between nearby luminescent impurities allows the excitation energy to non-radiatively decay; this non-radiative decay is most likely due to the presence of a nearby defect [15, 17].

Flux introduced into the CaS:Pb thin-film can increases luminance by acting as both a diffusing agent and a source of space charge. The first role of a flux in improving the performance of a CaS:Pb ACTFEL device is probably to enhance the mobility of Pb in the film, and thus encourage formation of Pb dimers necessary for blue EL emission. Flux-introduced donors are believed to create acceptor-like

calcium vacancies in the lattice [32, 33, 34]. The Pb ion probably diffuses by second nearest-neighbor hopping on cation sites. Therefore, additional calcium vacancies should increase the mobility of the lead ions by providing pathways for the diffusing impurity. Calcium vacancies are also responsible for positive space charge in the device. Space charge will enhance the phosphor field in portions of the phosphor and therefore induce a higher kinetic energy in the traversing electrons, meaning that more electrons will be energetic enough to excite the high energy blue transitions of Pb dimers.

Although both methods increase the brightness of evaporated CaS:Pb ACTFEL devices, co-evaporation of KCl or NaCl is found to be more effective than flux layer doping. Keir theorizes that in SrS films co-evaporation of KCl preferentially incorporates Cl into the film because of the formation of volatile K_2S [9]. Keir also asserts that flux layer doping of KCl is more likely to incorporate both Cl and K into the film since only a small amount of K_2S formation is likely to occur at the film surface. Although Keir's arguments were invoked to explain SrS fluxing trends, they should also apply to CaS. If Cl is incorporated into the CaS thin-film, it can substitutionally replace a sulfur ion and act as a donor. To maintain charge neutrality in an insulating material, donors must be compensated by a like number of acceptors. If a flux-introduced acceptor, like K, is not present, acceptors will most likely take the form of Ca vacancies. A flux dopant method such as KCl co-evaporation which preferentially adds Cl will therefore be more effective at creating Ca vacancies. Thus, co-evaporation of KCl (or NaCl) is expected to result in more mobile Pb and greater amounts of space charge than flux layer deposited KCl (or NaCl).

The luminance increase in sputtered CaS:Pb ACTFEL devices doped with KCl can also be attributed to an increase in calcium vacancies leading to a greater number of Pb dimers and space charge. The ineffectiveness of NaCl as a flux layer dopant may be a result of the small size of Na. Since Na is smaller than K it will be more likely to diffuse into the CaS:Pb film and incorporate into the lattice

along with Cl, adding both donors and acceptors to the phosphor film. Fewer unpaired Cl donors may mean less efficient vacancy creation and less mobility enhancement.

4.2.5 CaS:Pb Conclusions

The low brightness of the CaS:Pb ACTFEL devices studied is insufficient to warrant future investigation. The maximum brightness of the e-beam CaS:Pb ACTFEL devices prepared was 3.24 cd/m^2 @ 1 kHz, using a 3% evaporation ratio of $PbCl_2$ to CaS with a KCl co-evaporation. The maximum brightness of sputtered CaS:Pb ACTFEL devices measured was 4.99 cd/m^2 @ 1 kHz with a KCl flux layer. The brightness of CaS:Pb is believed to be limited at low lead concentration by the number of lead dimers formed and at high lead concentration by concentration quenching. Unless dimers can be preferentially formed even more efficiently than what is achieved using KCl co-evaporation, the brightness of this material is expected to remain low due to the trade off between dimer formation and concentration quenching.

4.3 BaS:Eu as an ACTFEL phosphor

4.3.1 Motivation for BaS:Eu

As mentioned in the previous $YVO_4 : Eu$ section, europium (Eu) has long been used as a red-emitting luminescent impurity for cathodoluminescent applications. $YVO_4 : Eu$, $Y_2O_2S : Eu$, and $Y(WO_3)_4 : Eu$ have already been discussed in Section 4.1. These phosphors luminesce via emission from the Eu^{3+} ion. The europium ion is also commonly found in the Eu^{2+} valence state. Typically trivalent Eu is found in host materials with a corresponding trivalent cation, such as Y^{3+}. Similarly, divalent Eu is found in host materials with divalent cations [75].

One of the most widely studied red-emitting EL materials, CaS:Eu, is based on the emission of Eu^{2+}. Eu^{2+} has a 5d $\rightarrow$ 4f luminescent transition giving it a

crystal field dependent emission spectrum (unlike Eu^{3+}). When Eu^{2+} is placed in the crystal field of a CaS lattice the ion produces red luminescence from a broad emission peak at 650 nm [76, 77]. The color and brightness of the $CaS : Eu^{2+}$ emission made it an intensely studied ACTFEL phosphor for some time [78, 79]. After much work, it was finally concluded that stability issues, in addition to the refractory nature of CaS, made this phosphor unattractive to pursue as an ACTFEL display material.

Barium sulfide, BaS, is an ACTFEL phosphor that may be appropriate as a Eu host. One of the attractive features of BaS is a relatively low melting temperature. The lower melting temperature aids in the manufacturability of the material for ACTFEL applications. The increased size of the BaS lattice compared to the CaS lattice translates into a reduction in the crystal field in BaS with respect to CaS. Theoretically, a change in crystal field should cause a shift in the emission spectra from a crystal field dependent substitutional luminescent impurity, like Eu^{2+}. If the crystal field is reduced, as is the case in the CaS to BaS transition, the emission from the luminescent impurity should shift to a higher energy emission [15, 16]. This section presents an investigation of BaS:Eu as a red ACTFEL phosphor which can be processed at a low annealing temperature.

4.3.2 BaS:Eu Sample Preparation

BaS:Eu ACTFEL devices are fabricated in the standard structure as discussed in Section 4.2.2. BaS is synthesized by Ben Clark and cold-pressed into BaS e-beam pellets. The BaS source material is formed from $Ba(CO_3)$ which is fired at 950°C for 2 hours with H_2S. The BaS e-beam pellets are sintered up to 1400°C. ITO/ATO coated glass is used as a substrate. An e-beam evaporated BaS film is co-evaporated with a EuS or EuF_3 dopant source. This structure is topped with a SiON thin-film insulator and a patterned aluminum layer.

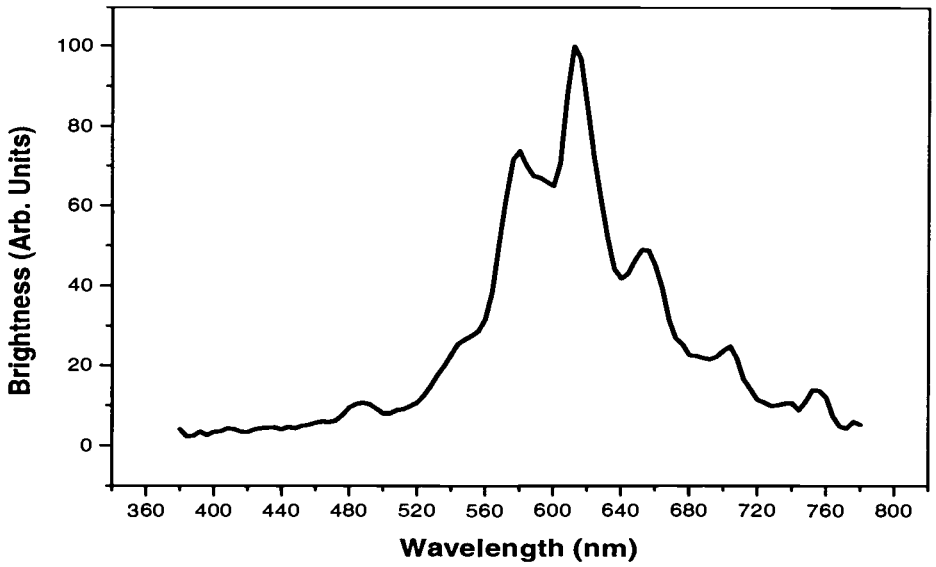

Figure 4.7. EL spectrum of a BaS:Eu ACTFEL device doped with EuS.

4.3.3 BaS:Eu Results

An EL spectrum from an e-beam evaporated BaS:Eu ACTFEL device is shown in Fig. 4.7. The europium source used as the thermal co-evaporant in this sample is EuS, chosen because of availability as well as matching of the Eu^{2+} valence to the Ba^{2+} valence. CIE coordinates for this BaS:Eu spectrum are (0.524, 0.417), which corresponds to an orange light emission.

It appears that the spectral features displayed in Fig. 4.7 are from both Eu^{2+} and Eu^{3+} emission. The large, relatively narrow, peak at 612 nm, which dominates the spectrum corresponds to emission from the Eu^{3+} ion. The shoulder at 580 nm is probably the principal Eu^{2+} emission, blue shifted in the BaS host from its position at 640 nm in CaS. The smaller side peaks at 545 and 655 nm are also due to Eu^{2+} emission, while the 705 nm peak is from the Eu^{3+} ion.

The EL spectrum shown in Fig. 4.8 is from another BaS:Eu ACTFEL device doped with EuF_3. The 612 nm peak of Eu^{3+} is clearly dominant. Two of the

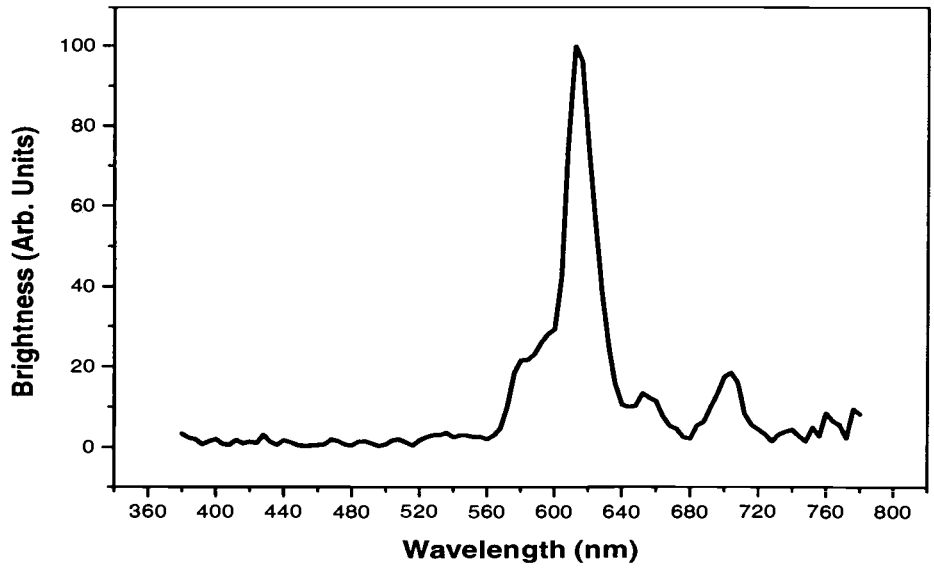

Figure 4.8. EL spectrum of a BaS:Eu ACTFEL device doped with EuF_3.

Eu^{2+} emission peaks, at 580 and 655 nm, are visible in Fig. 4.8, but their contribution is drastically reduced compared to the previous spectrum (Fig. 4.7). The CIE coordinates of the $BaS : EuF_3$ ACTFEL device of Fig. 4.8 are (0.616, 0.372), which are red-shifted from the spectrum shown in Fig. 4.7. Further optimization of red-emitting BaS:Eu using EuF_3 as a dopant source show a maximum luminescence at a evaporation ratio of 3% EuF_3 to BaS (from a study of 1% to 4%). The L_{40}, 60 Hz brightness of the best $BaS : Eu^{3+}$ ACTFEL device fabricated is 0.8 cd/m^2.

A C-V plot from a BaS:Eu ACTFEL device is shown in Fig. 4.9. This plot exhibits capacitance overshoot. As discussed in Section 3.2.3, C-V overshoot is evidence of dynamic space charge in the ACTFEL device. A device fabricated using KCl co-evaporation shows a reduction in this overshoot, as indicated in Fig. 4.10. This decrease in C-V overshoot was not accompanied by a major change in the emission characteristics; both devices have EL spectra similar to that shown in Fig. 4.8 and a L_{40} brightness of approximately 0.2 cd/m^2 @ 60 Hz.

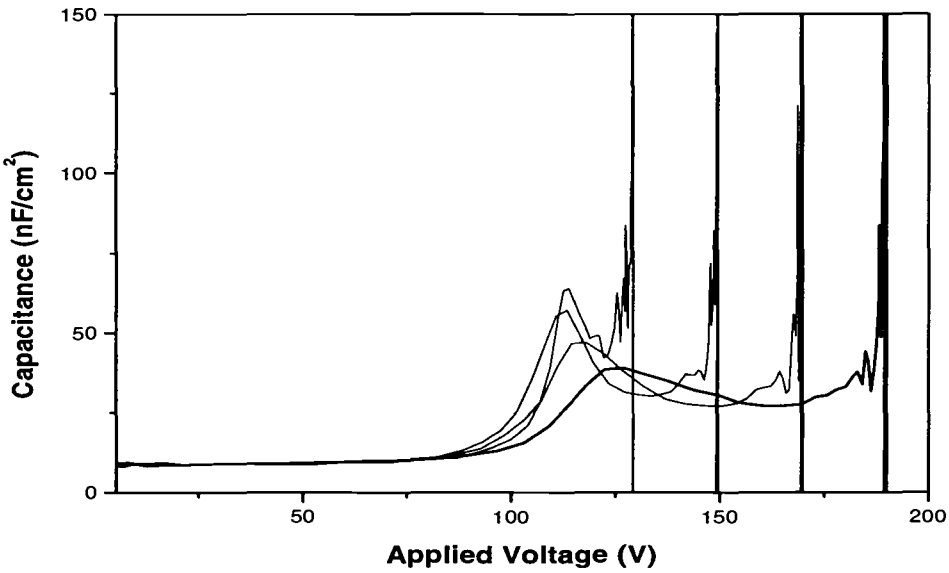

Figure 4.9. Capacitance-voltage plot of a BaS:Eu ACTFEL device using maximum applied voltages of 125, 145, 165, and 185 V.

4.3.4 BaS:Eu Discussion

A substitutional Eu ion sits on a cation site in the host lattice and will adopt the valence of the host cation that it replaces. In a BaS host the Eu ion will replace a Ba^{2+} cation and adopt a 2+ valence state. If the Eu ion is initally 3+ it will reduce to 2+ when substituted onto a Ba site [17, 80]. The most likely explanation for Eu^{3+} emission from BaS:Eu ACTFEL devices is the formation of a separate complex of Eu (for example EuF_3 or $EuCl_3$) within the BaS host. Eu^{3+} emission when EuF_3 is used as a dopant source suggests that Eu is incorporating in a non-substitutional manner, probably as a precursor complex of EuF_3. The observation of Eu^{3+} emission when EuS is used as a dopant source also indicates a non-substitutional incorporation, in this case it may be an impurity-related complex such as Eu_2O_3 or $EuCl_3$, although the source of oxygen, or other contaminant, is unclear. Assuming a contaminant is present the Eu^{2+} ion can be oxidized, so a Eu^{2+} dopant source does not preclude Eu^{3+} incorporation.

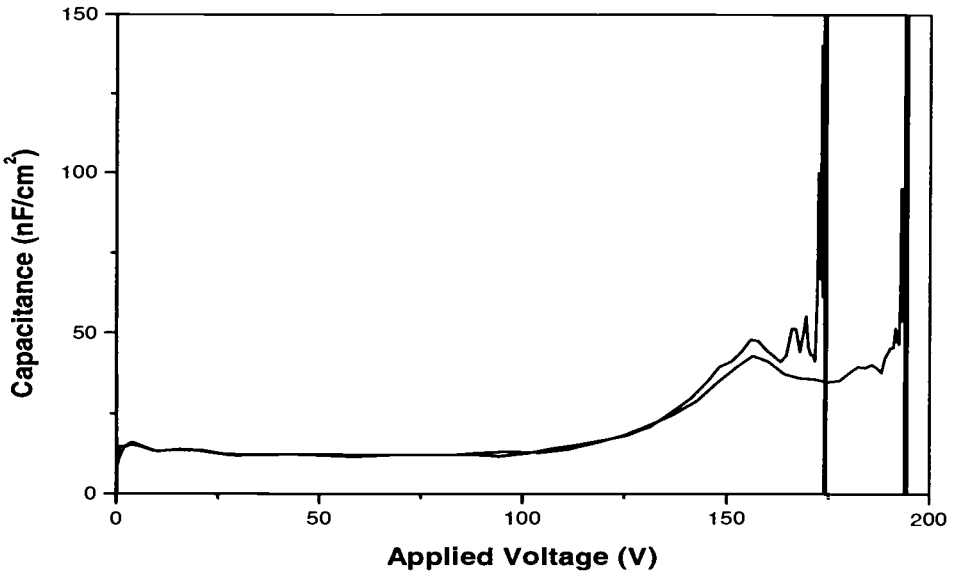

Figure 4.10. Capacitance-voltage plot of a BaS:Eu ACTFEL device co-evaporated with KCl using maximum applied voltages of 170, and 190 V.

Eu^{3+} EL emission is not observed in other sulfide hosts. For example, SrS ACTFEL devices, fabricated using a similar process do not display Eu^{3+} emission [81]. The major difference in thin-film deposition methodology between SrS:Eu and BaS:Eu is the temperature of processing. SrS:Eu thin-films are deposited at a substrate temperature of 300°C and are annealed at an RTA temperature of 810°C. BaS:Eu thin-films are deposited at a substrate temperature of $150° - 250°$C and annealed at an RTA temperature of 550°C and films RTAed at 810°C lose structural integrity. Perhaps the lower temperature used to crystallize the BaS host is insufficient to distribute and/or break up luminescent impurity precursors. If this is the case, the brightness of ACTFEL devices deposited at low processing temperatures would be enhanced if an activation energy, from the plasma in a sputtering or CVD process for example, is furnished to the forming film.

The reduction in C-V overshoot in the BaS:Eu ACTFEL devices deposited using co-evaporation of KCl (illustrated in Figs. 4.9 and 4.10) indicates that KCl

co-evaporation results in a reduction of space charge. As mentioned in Section 4.2.4, co-evaporation of KCl results in a preferential incorporation of Cl donors into the film due to a reaction which produces volatile K_2S. Cl donors incorporated into the film may be diffusing to the boundaries between the BaS lattice and the Eu sub-lattice. It is likely that numerous defects surround these Eu sub-lattice sites, and the introduction of Cl may fill some of the vacancies and reduce the number of local electron traps.

4.3.5 BaS:Eu Conclusions

Red BaS:Eu ACTFEL devices have good color coordinates and an attractive low 550^{o}C annealing temperature. However, the low brightness of 0.8 cd/m^2 @ 60 Hz achieved in this study, and the existence of Eu^{3+} emission suggests that these devices are non-optimized. Possible ways to improve the BaS:Eu ACTFEL performance include fluxing to better incorporate Eu into the BaS host or the use of activated deposition to improve Eu incorporation into BaS.

4.4 SrS:Er,Gd as an ACTFEL phosphor

4.4.1 SrS:Er,Gd Motivation

Erbium, a member of the lanthanide series of rare earth elements, is an atom which, similar to Eu^{3+}, exhibits luminescence from an intra-shell 4f $\rightarrow$ 4f transition. As previously mentioned, a 4f $\rightarrow$ 4f luminescent transition is shielded from the crystal field by outer 5s and 5p electron shells [15, 17]. Electron shielding minimizes the ACTFEL host's influence on the spectrum of the luminescent impurity. That said, the existence of high energy peaks in the EL spectrum of Er may still be host-dependent since energetic electrons must be available in the host in order to excite high energy luminescent transitions.

Evidence has been presented that SrS is a better ACTFEL host material for blue emitting luminescent impurities than ZnS, due to a higher concentration of

hot-electrons. [82, 83]. Erbium-doped zinc sulfide has a spectra which mainly consists of peaks at 530, 550, and 660 nm [84, 85]. The SrS:Er spectrum is similar to ZnS:Er but also exhibits an additional high energy peak at 380 nm [83, 86]. Recent work by Keir *et al.* shows a comparison of the spectra in both ZnS and SrS hosts [82]. His results, which support previous findings, show that the green emission which erbium produces in ZnS [CIE coordinates (0.309,0.652)] is blue-shifted to a greenish-blue color in SrS with CIE coordinates (0.284,0.580) and a L_{40} brightness of 10.21 fL (34.98 cd/m^2) @ 1 kHz.

Gadolinium, like lead, is known to emit UV to blue light when incorporated as a luminescent impurity in a phosphor [15]. Wickerscheim and Lefever, and later D'Silva and Fassel, report 315 nm emission from Gd^{3+} [87, 88]. A precedent for Gd as an EL luminescent impurity has been set by Young-Jae Cho *et al.* who describe an ACTFEL device which uses the UV emission of SrS:Gd to excite PL from a second material [68]. After extensive optimization of the SrS:Gd UV emitter, they concluded that a $GdCl_3$ gadolinium source results in the most intense UV emission.

As previously discussed in Section 2.5, a luminescent impurity can be used for energy transfer in a phosphor film. The example given was the pumping of Eu^{2+} emission in CaS by the additional doping of Ce^{3+}. Excited Ce^{3+} ions may emit high energy photons which can be absorbed by the Eu^{2+} impurity, the energy of which can be subsequently re-emitted from the Eu^{2+} ion as red light (a lower energy photon). Gd^{3+}, with its UV emission, is a good candidate for a luminescent co-activator to pump the emission of a second luminescent impurity.

The blue EL emission of Gd may improve the chromaticity of the greenish-blue Er EL emission, while the UV EL emission from Gd may increase the brightness. In order to verify this supposition, SrS ACTFEL devices doped with both Er and Gd are fabricated.

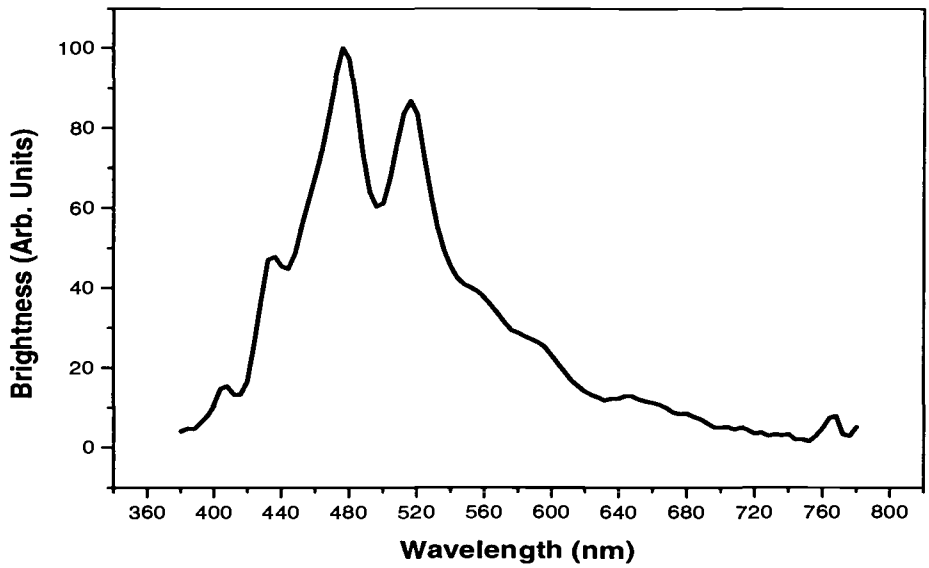

Figure 4.11. EL spectrum of a SrS:Gd ACTFEL device.

4.4.2 SrS:Er,Gd Sample Preparation

SrS:Er,Gd samples are fabricated as standard ACTFEL devices similarly to the CaS:Pb devices of Section 4.2.2. SrS pellets are synthesized by Ben Clark of the OSU Chemistry Department from a strontium carbonate source which is fired at 1200°C for five hours, then cold-pressed and sintered up to 1400°C. The SrS:Er,Gd phosphor layer is deposited via a two step sequence. The SrS pellet is e-beam evaporated concurrent with the thermal evaporation of ErF_3. After the phosphor layer has been deposited a thin-film of the gadolinium source is deposited on half or all of the sample and is then fluxed into the SrS:Er film during a 2 1/2 minute RTA anneal at 810°C. Observation of two distinct PL colors from a sample which was half fluxed with $GdCl_3$ confirms that Gd is being incorporated into the film on one half of the sample.

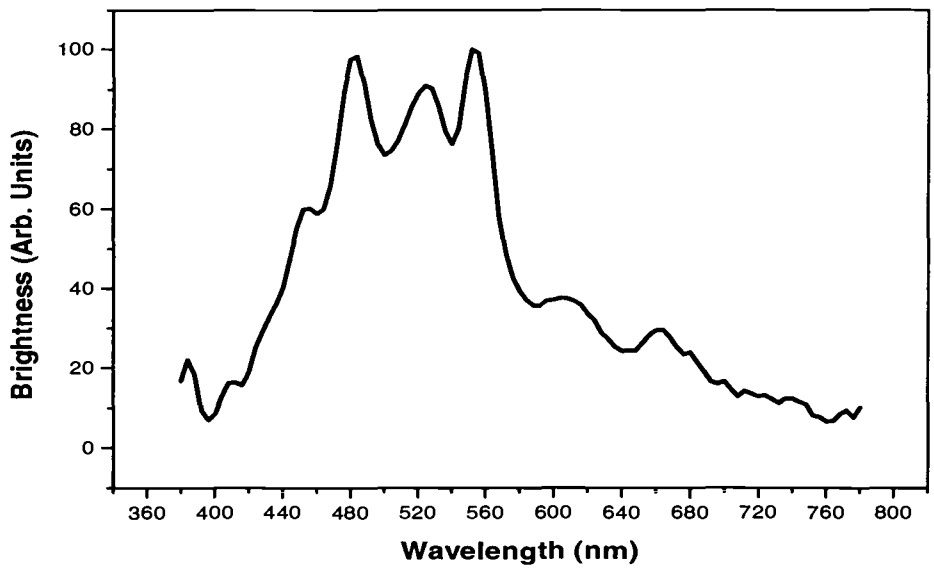

Figure 4.12. EL spectrum of a SrS:Er ACTFEL device.

4.4.3 SrS:Er,Gd Results

The EL spectrum of a SrS:Gd ACTFEL device, fabricated by co-evaporation using $GdCl_3$ as a Gd source is shown in Fig. 4.11; this spectrum is obtained using the standard PR650 spectro-photometer used in the rest of this thesis work. UV emission from the SrS:Gd ACTFEL device is measured by Beau Baukol using a photo-multiplier tube and a monochromator. A UV peak is found in the SrS:Gd EL spectrum at 315 nm. The SrS:Gd spectrum of Fig. 4.11 shows a dominant 476 nm emission, with smaller high energy peaks at 410 nm and 435 nm and a green peak at 515 nm. The CIE coordinates of this SrS:Gd ACTFEL device are (0.235, 0.326) and the L_{40} brightness is 14.93 cd/m^2 @ 60 Hz. $GdCl_3$ is used as the Gd source in the majority of samples fabricated. The choice of Gd dopant source is based on the work of Cho *et al.* who assert that $GdCl_3$ results in stronger UV emission than any of the other Gd sources investigated (i.e. $GdCl_3$, GdF_3, Gd_2O_3, and Gd_2S_3) [68].

For comparison purposes, the EL spectrum of a SrS:Er and a SrS:Er,Gd ACTFEL device from the same substrate are presented. A SrS:Er phosphor layer is deposited by co-evaporation of SrS and ErF_3. A flux layer of $GdCl_3$ is then deposited on one half of this sample, resulting in two active areas on the sample with only the $GdCl_3$ impurity differing between the two. The spectrum of an ACTFEL device from the SrS:Er side (no Gd) is shown in Fig. 4.12. Emission consists of spectral peaks at 480, 525, and 552 nm which give the device a greenish-blue color with CIE coordinates (0.277, 0.390). An unoptimized L_{40} brightness of 1.7 cd/m^2 @ 60 Hz is obtained from this SrS:Er ACTFEL device. A spectrum from an ACTFEL device on the same sample which has the additional $GdCl_3$ flux layer, is shown in Fig. 4.13. The spectral peaks of the Gd-enhanced device are now 410, 430, 480, and 530 nm, producing a much bluer emission with CIE coordinates (0.208, 0.235). The L_{40} brightness of the SrS:Er,Gd ACTFEL device is 1.5 cd/m^2 @ 60 Hz (again unoptimized), similar to the SrS:Er device.

Optimization of the brightness and the chromaticity of a SrS:Er,Gd ACTFEL device is based on a concentration study of both Er and Gd. A maximum brightness of 3.65 cd/m^2 @ 60 Hz is measured from a sample with an evaporation ratio of 0.5% Er to SrS and a flux layer of 1% $GdCl_3$. This sample had improved blue chromaticity, with CIE coordinates (0.17, 0.23).

4.4.4 SrS:Er,Gd Discussion

The EL spectrum of a dual-doped SrS:Er,Gd ACTFEL device has much bluer chromaticity than the spectrum of either of the constituents. The spectral peak at 480 nm is present in both the SrS:Er and the SrS:Gd ACTFEL devices and constitutes a significant portion of the SrS:Er,Gd spectrum. A major factor in the blue-shift observed in SrS:Er,Gd ACTFEL devices compared to both SrS:Er and SrS:Gd is the large spectral peak at 430 nm. This peak corresponds to the SrS:Gd 430 nm peak, and perhaps also has some contribution from the SrS:Er 450 nm peak. In addition, the lower wavelength peaks near 410 nm, which are quite

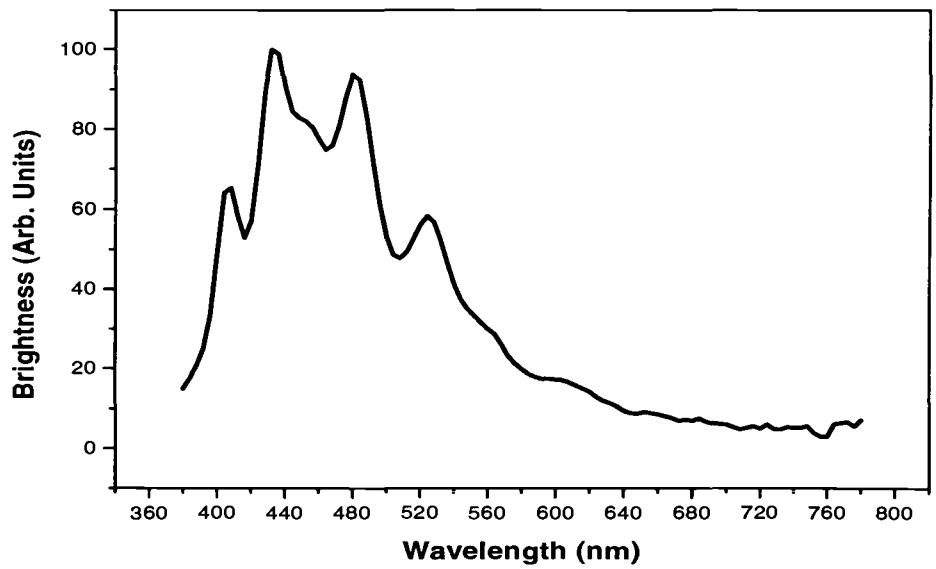

Figure 4.13. EL spectrum of a SrS:Er,Gd ACTFEL device.

small for both SrS:Er and SrS:Gd, combine to form a significant 410 nm peak in a SrS:Er,Gd ACTFEL device. What is not readily apparent is whether the UV emission from Gd^{3+}, which was the initial motivation for Gd as a luminescent co-activator, is a positive factor in the SrS:Er,Gd ACTFEL device.

One of the major problems with these devices is stability. Devices are susceptible to burn-out spots and a slow ramping voltage was required during testing to prevent device failure. However, the stability issues are likely to be process-related and further study may result in the fabrication of more stable devices.

4.4.5 SrS:Er,Gd Conclusions

Investigation of SrS:Er,Gd ACTFEL devices has resulted in several characteristics that deserve further study. A proof of concept has been presented for improved chromaticity of blue emission from an ACTFEL device when an additional Gd^{3+} luminescent impurity is added to the film. Further study of Gd as a

co-activator in other blue ACTFEL phosphor materials may also be fruitful. The SrS:Er,Gd ACTFEL device may also find use as one component in a white colored ACTFEL device, due to its broad blue emission.

Problems with the SrS:Er,Gd material include chromaticity and stability. The non-ideal blue chromaticity will limit direct applications of SrS:Er,Gd ACTFEL devices in full color displays. Issues of stability are also of concern since burn-out problems may be inherent to the material.

It is unclear at this point whether the UV emission from Gd is having a positive effect on the emission of SrS:Er,Gd. Future work could involve devising a method to test whether the UV portion of the gadolinium emission is having any pumping effect on the erbium emission.

4.5 Holmium Doping Study

4.5.1 Motivation for Holmium Doping

The ability of an ACTFEL phosphor host material to excite blue, i.e. high energy, EL is dependent on the availability of high energy electrons. Evaluation of the energy distribution of electrons in a host, and specifically the high energy electron distribution, is therefore invaluable in assessing the fitness of a material for use as an ACTFEL phosphor host.

One such electron distribution evaluation technique has been described by Keir *et al.* [82]. This technique consists of fabricating a series of ACTFEL devices with one phosphor host material doped with different 4f $\rightarrow$ 4f intra-shell lanthanide luminescent impurities; namely Er, Dy, Ho, Tb, and Tm and observing the emission from the shielded transitions. Since the 4f electron shell is shielded from the effects of the crystal field in the host lattice by outer 5s and 5p electron shells, the existence or absence of high energy spectral peaks is dependant on the relative high-energy electron distributions in the different host materials and branching ratios [82, 83].

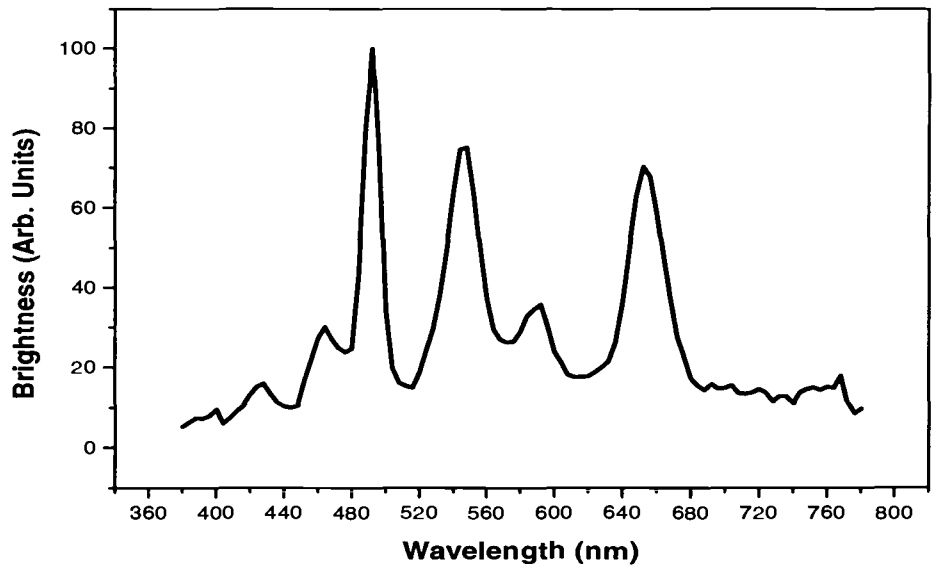

Figure 4.14. EL spectrum of a BaS:Ho ACTFEL device.

Keir's study compared lanthanide emission in ZnS and SrS ACTFEL phosphor hosts. The differences seen, mainly a suppression of high energy peaks in ZnS when compared with SrS, indicate a deficiency in high energy electrons in the ZnS host. The following is an extension of this study which investigates an additional series of phosphor host materials in order to evaluate their suitability as ACTFEL hosts. Holmium (Ho) is used as the lanthanide luminescent impurity in this study based on its abundance of high energy EL emission peaks.

4.5.2 Holmium Sample Preparation

BaS, CaS, and CaSe ACTFEL devices are fabricated in the same manner as devices from Keir's study [82]. BaS and CaS source materials are formed from their respective carbonates and are annealed in an H_2S environment at 960°C and 1200°C respectively for 2 hours. Pellets are then cold-pressed and sintered up to 1400°C. CaSe pellets are cold-pressed from CaSe source material from Cerac,

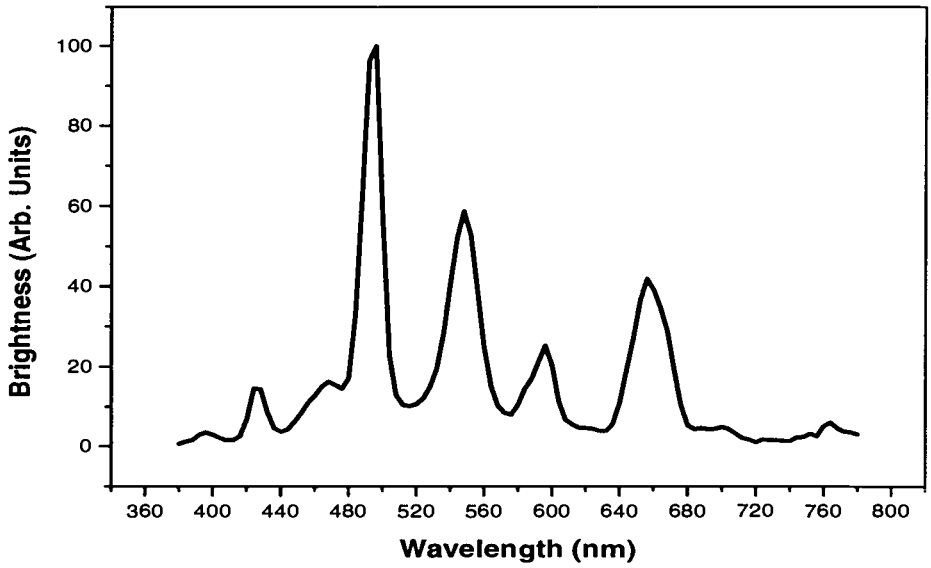

Figure 4.15. EL spectrum of a CaS:Ho ACTFEL device.

Inc., and sintered up to 1400°C. BaS, CaS, and CaSe pellets are then e-beam evaporated with a thermal co-evaporation of HoF_3. The Ho/sulfide evaporation ratio is 0.75%. The remainder of the device is the standard ACTFEL structure discussed in Section 4.2.2, with ITO/ATO, bottom conductor/bottom insulator thin-films, and SiON/Al, top insulator/top conductor thin-films.

4.5.3 Holmium Doping Results and Discussion

The EL spectrum measured from BaS:Ho, CaS:Ho, and CaSe:Ho ACTFEL devices are shown in Figs. 4.14, 4.15, and 4.16, respectively. The EL spectra from BaS:Ho and CaS:Ho ACTFEL devices (Figs. 4.14 and 4.15) both show a dominant spectral peak at 490 nm with smaller, higher energy spectral peaks visible at 425 and 465 nm. Lower energy emissions are seen at 550, 595, and 660 nm. The spectra of BaS:Ho and CaS:Ho match that of a SrS:Ho ACTFEL device measured in Keir's study [82]. The ACTFEL hosts BaS and CaS, therefore, appear

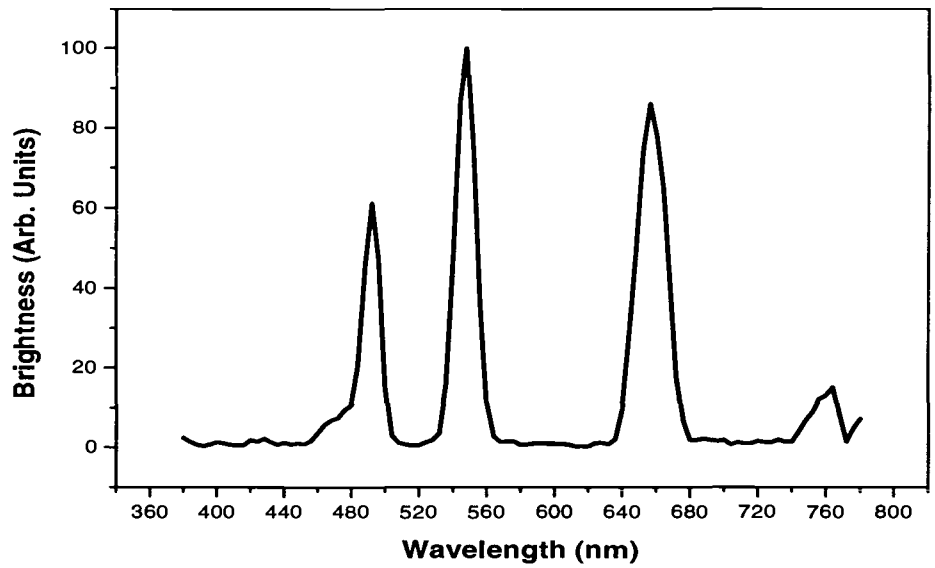

Figure 4.16. EL spectrum of a CaSe:Ho ACTFEL device.

to have adequately heated hot-electron distributions so that these phosphors are appropriate for blue ACTFEL phosphor applications

In contrast, the EL spectrum from a CaSe:Ho ACTFEL device (Fig. 4.16) shows a definite suppression of the high energy portion of the Ho spectrum. The 490 nm peak, while still visible, is no longer dominant. Additionally, the other high energy peaks are not visible in the CaSe spectrum. The lower energy peaks at 550 and 660 nm are visible, and indeed dominate this spectrum. However, the spectral peak at 595 nm is absent. The 595 nm Ho peak is attributed to the $^5G_4 \rightarrow {}^5I_6$ electron state transition. This relatively long wavelength emission involves luminescent decay from one high energy state to a second high energy state. Therefore, this transition is only evident when high energy electrons are present to excite it. The absence of the 595 nm spectral peak is strong evidence that the differences seen between CaSe and other ACTFEL host materials are not merely branching ratio issues, but rather hot-electron deficiencies. The CaSe:Ho spectrum is similar to the ZnS:Ho ACTFEL device spectrum in Keir's study [82],

although the high energy portion of the spectrum is not as depressed in the CaSe host as it is in the ZnS host. Therefore, CaSe appears to be a poor choice as an ACTFEL phosphor for short wavelength (high energy) light emission because the hot-electron distribution is inadequately heated.

4.5.4 Holmium Doping Conclusions

This study provides further evidence for the viability of the lanthanide-doping method for determining the relative high energy portion of the electron distribution in an ACTFEL host material. A comparison of spectra from Ho-doped BaS, CaS, and CaSe ACTFEL devices shows that BaS and CaS have more high energy EL emission than CaSe. This is attributed to a more heated hot-electron distribution in BaS and CaS hosts compared to CaSe. Thus, this result indicates that BaS and CaS are more appropriate blue-emitting ACTFEL hosts than CaSe. Combining these results with those of Keir *et al.*, BaS, CaS, and SrS appear to have adequately heated electron distributions for blue ACTFEL device applications, whereas CaSe and ZnS do not [82].

4.6 Additional ACTFEL phosphors

4.6.1 BaS ACTFEL phosphors

BaS is an infrequently studied ACTFEL phosphor host because of its poor performance in other display technologies. In an attempt to obtain a general overview of BaS as an ACTFEL host material, a series of BaS ACTFEL devices with various luminescent impurities are evaluated.

The series of ACTFEL devices fabricated consists of BaS doped with Mn, Pb, Ag, and Sn. EL spectra for these films are shown in Figs. 4.17, 4.18, 4.19 and 4.20. These ACTFEL device spectra have EL emission between 560 and 580 nm, with a resulting orange light. An EL spectrum from an undoped BaS film

is shown in Fig. 4.21. The undoped device emission is dominated by a 560 nm peak.

This series of luminescent impurities usually emit from red to blue in other ACTFEL hosts. Thus, the dominant orange emission found in all of these BaS devices is unexpected. The origin of this orange emission in doped and undoped BaS is unclear. One possible cause is an electron distribution which maximizes at 560 nm and is deficient in the blue portion of the spectrum. However, the Ho doping study of Section 4.6 excludes this as a possibility.

A second possible cause of orange EL emission in BaS is a non-linear crystal-field effect. A blue-shift is expected with increasing lattice size, since a substitutional impurity ion will experience a lower crystal field. A red-shift is expected with increasing covalency between a substitutional luminescent impurity and the surrounding ligands (called the nephelauxetic effect) [89].

As an example of the nephelauxetic effect, O'Brien *et al.* theorize that the red-shift seen between the EL emission of SrS:Ce and BaS:Ce is a product of an increased covalency between the Ce luminescent impurity and S ligands in the BaS lattice, with respect to that same ligand bond in the SrS lattice [90]. Perhaps either increasing lattice size, or the nephelauxetic effect is at work in each BaS spectrum, shifting the spectrum either red or blue with a net result of orange emission from all the BaS spectra. This seems a highly unlikely explanation for the orange emission from BaS ACTFEL devices since the emission spectra is so consistently centered at 560-580 nm. Additionally color-shifts compared to other sulfide emissions, do not follow size trends, such as smaller impurity atoms being susceptible to the nephelauxetic effect and red-shifting and larger impurity atoms blue-shifting in accordance with larger lattice parameters.

Another, more likely, source of orange EL emission from BaS ACTFEL devices is an intrinsic defect or copper contamination in the film. The undoped BaS ACTFEL device EL spectrum supports this hypothesis, since it also exhibits a 560 nm peak. However, undoped BaS emission is very dim and tends to fade

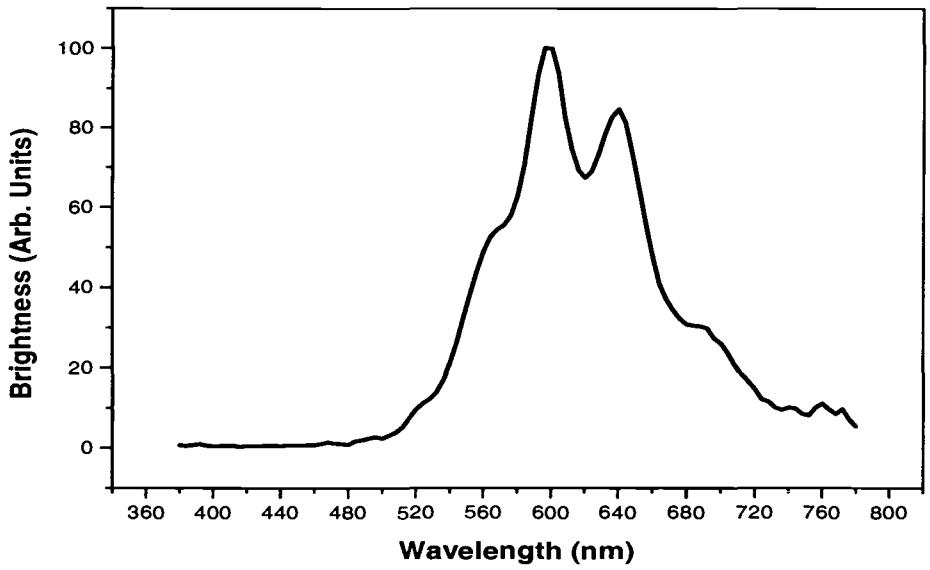

Figure 4.17. EL spectrum of a BaS:Mn,KF ACTFEL device.

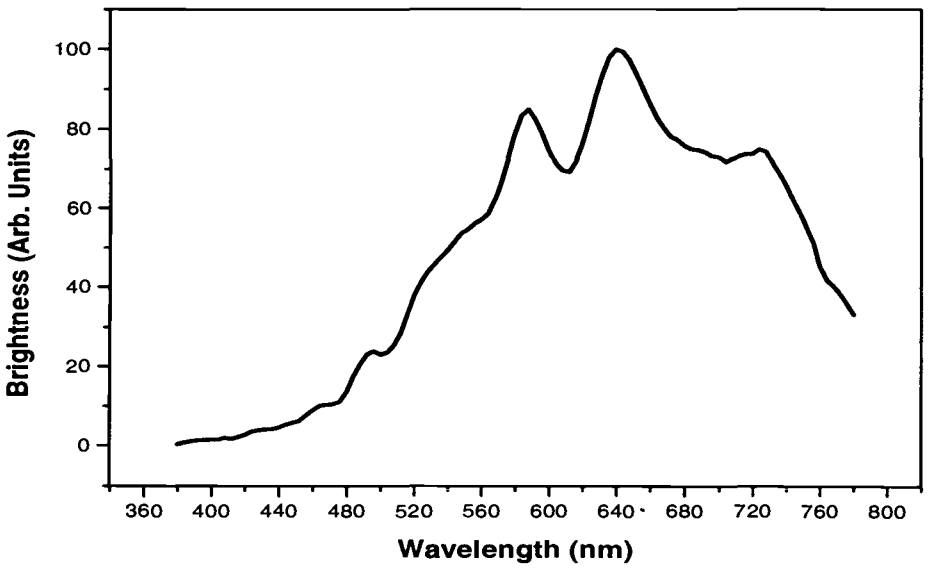

Figure 4.18. EL spectrum of a BaS:Pb ACTFEL device.

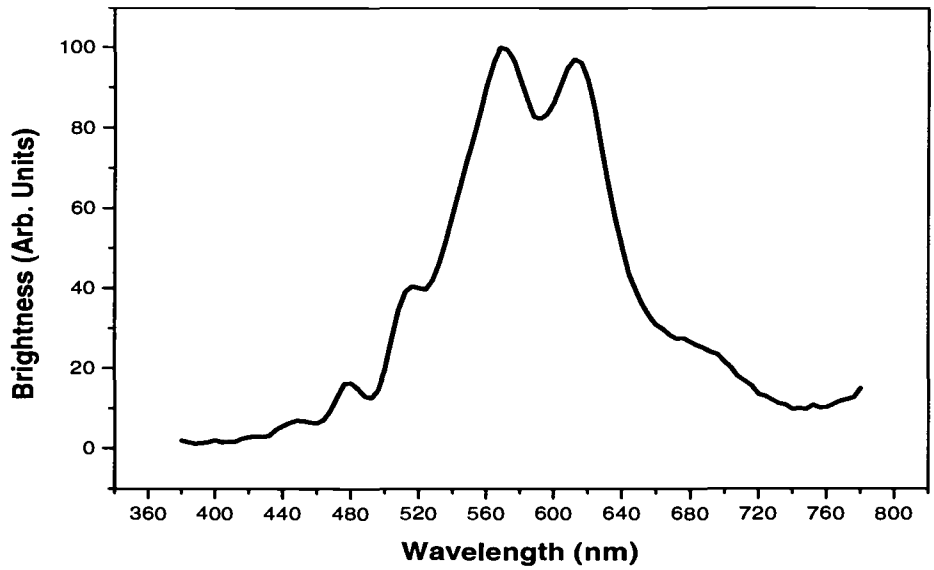

Figure 4.19. EL spectrum of a BaS:Sn ACTFEL device.

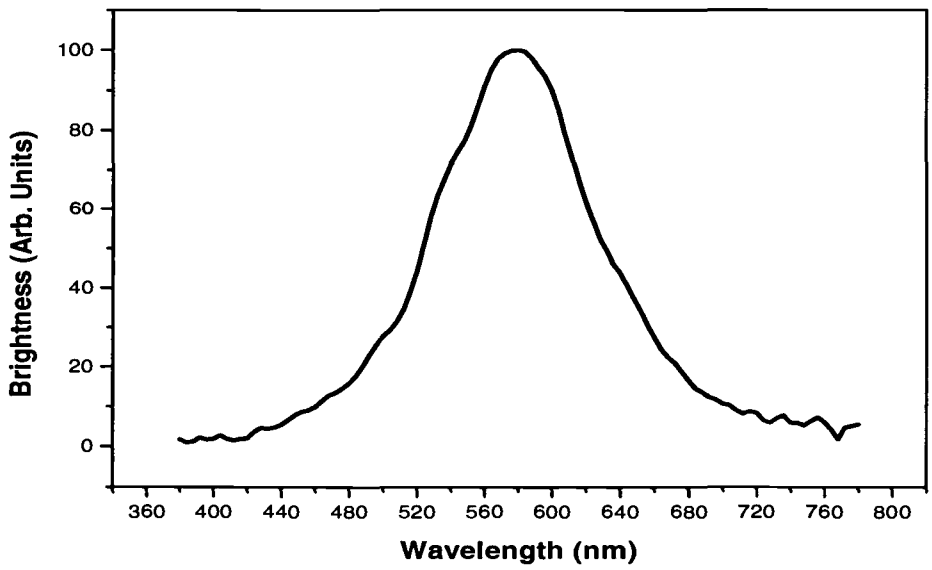

Figure 4.20. EL spectrum of a BaS:Ag ACTFEL device.

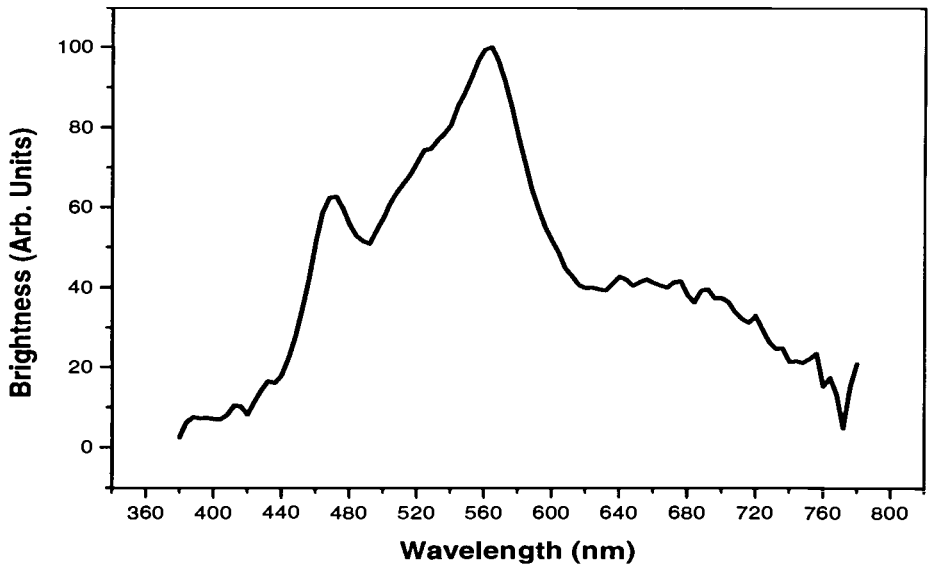

Figure 4.21. EL spectrum of an undoped BaS ACTFEL device.

to below measurable levels with short aging times. Thus, if an intrinsic defect or copper contamination is the source of orange emission it is being somehow enhanced by the introduction of a luminescent impurity into the film.

4.6.2 CaS:Sm as an ACTFEL phosphor

Trivalent samarium (Sm^{3+}) is a lanthanide ion which emits in the red portion of the spectrum. Co-evaporation of CaS and SmF_3 at a substrate temperature of 300°C and an RTA temperature of 810°C produces an ACTFEL device with the EL spectrum shown in Fig. 4.22 and an L_{40} brightness of 3.58 cd/m^2 @ 60 Hz. The chromaticity (0.524, 0.431) of the spectrum shown in Fig. 4.22 is poor compared to the red ACTFEL device goal of (0.6, 0.3).

The most interesting result of an investigation of this material involves flux layer doping with NaF. CaS is a refractory compound which typically requires annealing temperatures of 800°C or more for proper crystallization. A fluxed

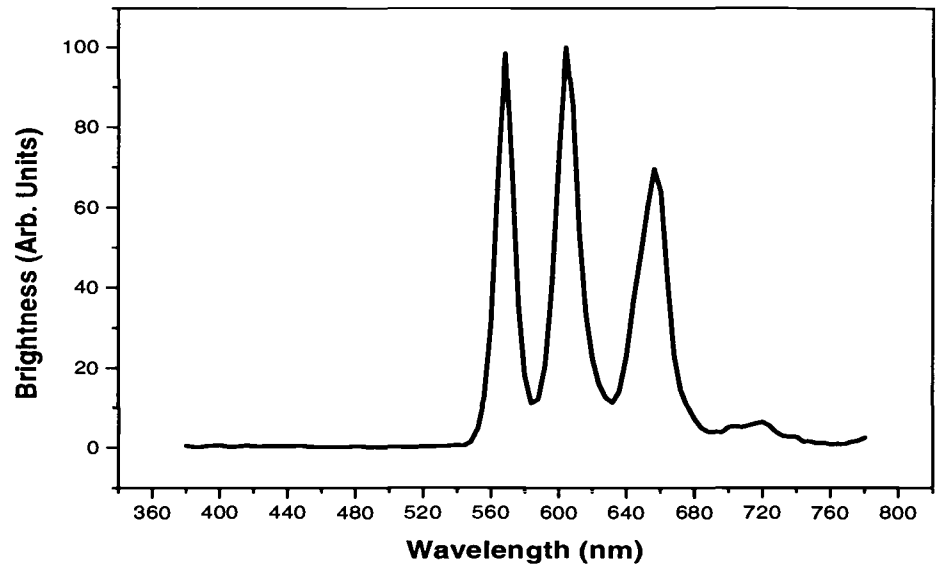

Figure 4.22. EL spectrum of a CaS:Sm ACTFEL device.

CaS:Sm,Na ACTFEL device RTAed at 810°C (the same anneal temperature of the unfluxed sample from above) experiences a three-fold increase in L_{40} brightness to 10.57 cd/m^2 @ 60 Hz. The increase in brightness is attributed to an increase in crystallinity in CaS, and EL emission is found to occur at a temperature as low as 650° C. A fluxed CaS:Sm,Na ACTFEL device RTAed at 650°C has an L_{40} brightness of 3.16 cd/m^2 with the same spectral peaks as shown in Fig. 4.22. Note that both flux constituents Na^{1+} and F^{1-} are relatively small ions, and as such are probably efficient flux agents. A NaF flux layer may be useful in enhancing crystallinity in CaS thin-films doped with other luminescent impurities and used as ACTFEL phosphors, that were previously discarded due to high temperature requirements.

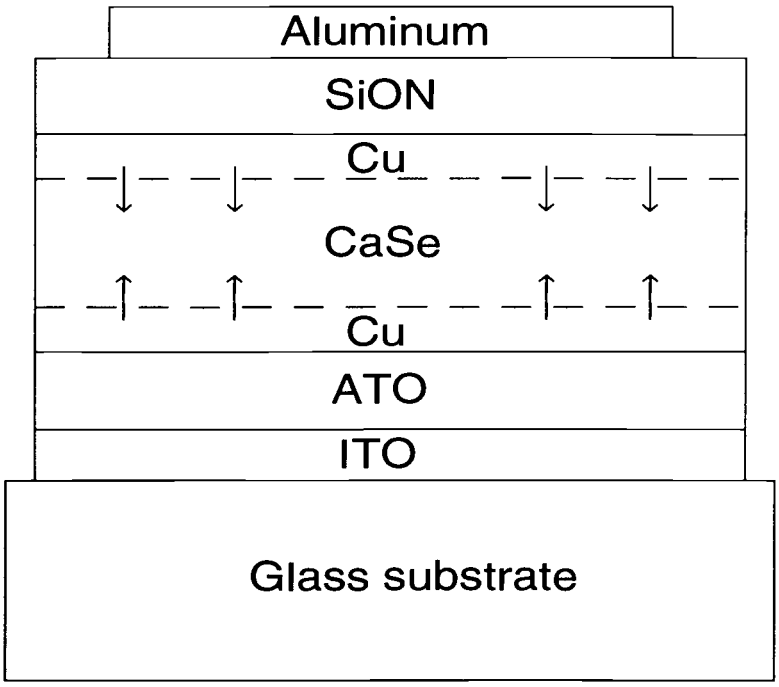

Figure 4.23. Phosphor sandwich fluxing technique.

4.6.3 CaSe:Cu as an ACTFEL phosphor

The chromaticity of EL emission from the Cu ion is dependent on the ACTFEL host into which it is substituted. BaS:Cu as an ACTFEL phosphor emits at approximately 580 and 620 nm [9]. EL emission from SrS:Cu occurs with peaks at approximately 465 and 490 nm [9]. A CaS:Cu ACTFEL device fabricated prior to this study exhibits dominant EL emission at 456 nm with a significant side peak at 505 nm. The general trend is that the spectrum shifts in the blue direction as the host changes from BaS to SrS to CaS, corresponding to a decrease in lattice size and an increase in crystal field. CaSe has a lattice constant of 0.5927 nm, which falls between the lattice constants of SrS (0.6019 nm) and CaS (0.5697 nm), this means that the emission spectrum of CaSe:Cu should also fall between that of SrS:Cu and CaS:Cu [15]. In order to test the theorized blue emission of CaSe:Cu, ACTFEL devices are fabricated using a phosphor sandwich technique,

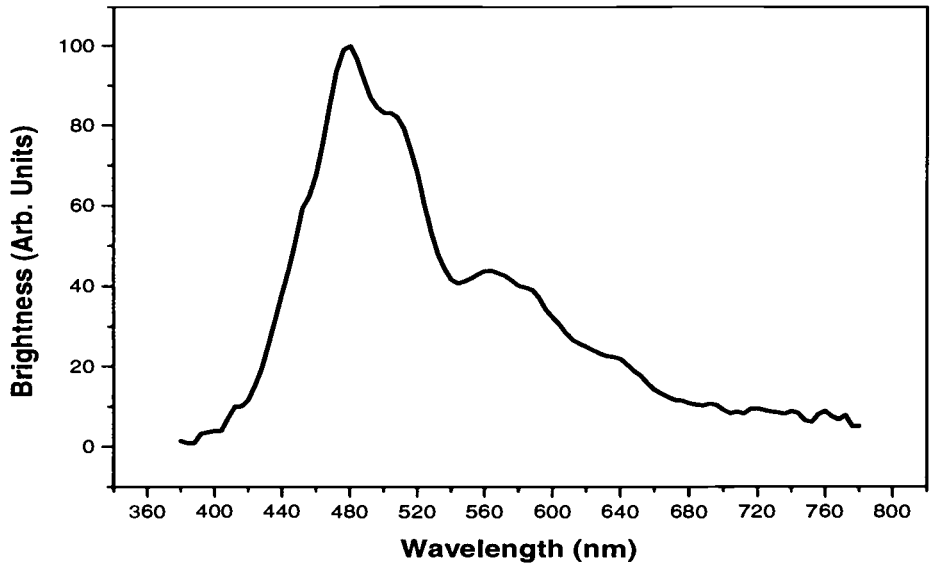

Figure 4.24. EL spectrum of CaSe:Cu ACTFEL device.

as illustrated in Fig. 4.23. In this technique a thin layer of a copper compound is first thermally evaporated onto the ITO/ATO substrate. Next, the CaSe film is deposited on top of the first copper compound layer. Finally, a second thin, thermally evaporated, layer of the copper compound is deposited. The resulting thin-film stack is shown in Fig 4.23. When the device is RTAed, copper ions diffuse from the copper compound layers into the CaSe film. This method of introducing impurities into a phosphor layer is more reproducible than the co-evaporation method [9].

The EL spectrum from a CaSe:Cu ACTFEL device is shown in Fig. 4.24. The EL spectrum consists of a dominant emission at 480 nm with a shoulder at around 505 nm, and a second peak at 560 nm. This second peak is often significant in the spectrum. The CaSe:Cu ACTFEL device gives very dim blue emission of 2 cd/m^2 @ 5 kHz.

The dominant 480 nm peak in CaSe:Cu falls between the 490 nm peak of SrS:Cu and the 437 nm peak of CaS:Cu. This was the theorized result from the

CaSe host, which is between SrS and CaS in size. The origin of the 560 nm peak is unclear.

The Ho-doping study of Section 4.6 brings to light a deficiency in the high energy electron distribution in the CaSe material. The low concentration of high energy electrons with which to excite blue EL and the resulting dim blue light output suggests that CaSe:Cu is probably not a viable blue ACTFEL phosphor. The correlation between results of the Ho-doping study from Section 4.6 and the poor blue EL emission from CaSe:Cu is added evidence of the utility of the lanthanide doping method in predicting good blue EL host materials.

Chapter 5
Conclusions/Recommendations for Future Work

5.1 Conclusions

A number of ACTFEL material systems have been investigated and several scenarios are proposed to explain some of their properties. Materials studied include $YVO_4 : Eu$, CaS:Pb, BaS:Eu, SrS:Er,Gd, BaS doped with various luminescent impurities, CaS:Sm, CaSe:Cu, and BaS, CaS, and CaSe doped with holmium.

- $YVO_4 : Eu$

  A well known red CL phosphor with bright PL, $YVO_4 : Eu$ appears to have poor charge injection and transport characteristics as an ACTFEL device.

- CaS:Pb

  Dim blue EL emission is observed from CaS:Pb ACTFEL devices. This poor EL performance is probably due to an inadequate number of dimer complexes formed at low Pb concentrations and concentration quenching at high Pb concentrations.

- BaS:Eu

  BaS:Eu ACTFEL devices fabricated show dim red EL emission arising from both Eu^{2+} and Eu^{3+} ions. Eu^{3+} emission is not expected for Eu substitution onto a Ba^{2+} cation site; thus Eu^{3+} emission probably originates from impurity- or precursor-related complexes. It is suspected that this impurity- or precursor- related complex formation occurs because of the relatively low deposition and RTA temperatures used in BaS thin-film synthesis.

- SrS:Er,Gd

  The addition of Gd causes a blue shift in the spectrum of a SrS:Er ACTFEL device resulting in emission at CIE coordinates (0.208, 0.235). This blue shift is due to the enhancement of short wavelength peaks arising from Gd emission. Additionally, part of this blue-shift could be due to Gd-induced UV pumping of blue EL emission since Gd emits in the UV at 315 nm.

- Ho-doping

  By comparing the strength of high energy peaks of Ho doped into ACTFEL host materials it is found that BaS and CaS have hot-electron distributions energetic enough to induce blue EL emission. Furthermore, it is shown that the hot-electron distribution in CaSe is less energetic than BaS or CaS and is therefore not a good blue EL host material.

- BaS:X

  The EL spectra of BaS ACTFEL devices doped with Mn, Pb, Sn, and Ag as luminescent impurities all display orange emission. This is probably due to unintentional Cu contamination or the formation of an intrinsic defect.

- CaS:Sm

  A threefold improvement in brightness (from 3.58 to 10.57 cd/m^2 @ 60 Hz) with the fluxing of NaF into CaS:Sm ACTFEL devices is observed with an RTA temperature of 810°C. Of more interest however, is a brightness of 3.16 cd/m^2 which is obtained from a NaF fluxed CaS:Sm ACTFEL device RTAed at a temperature of 650°C. CaS:Sm emission is red with typical CIE coordinates (0.524, 0.431).

- CaSe:Cu

  CaSe:Cu is shown to be a poor blue ACTFEL phosphor. Its weak EL performance is attributed to an inadequately heated hot-electron distribution, as deduced from Ho doping studies.

5.2 Recommendations for Future Work

Additional research related to the following topics is warranted:

The poor EL performance of BaS:Eu ACTFEL devices is attributed to complexes forming because of low deposition and RTA temperatures. These low processing temperatures are believed to result in increased incorporation of undesirable impurities into the thin-film. This may be due to the higher sticking coefficient of a surface at a lower temperature, as well as the fact that an adsorbed precursor species is less likely to dissociate at a lower temperature. Therefore, future work should explore the use of activated deposition methods (e.g. sputtering, ion-assisted deposition, activated evaporation) to more efficiently incorporate Eu, or other luminescent impurities, into the BaS thin-film without introducing undesirable impurities. Since a higher RTA temperature does not appear to be optimal for BaS, it may be desirable to increase the deposition temperature and keep the RTA temperature low, as most of the impurities are likely to be incorporated during thin-film deposition. The challenge is to maintain thin-film integrity as well as the low-temperature processing advantages of BaS, but simultaneously improve the BaS EL performance. Further investigation of the BaS host is also needed to fully understand the source of the dominant orange emission.

Gd doping of SrS:Er leads to a variety of possible future experiments. Additional research needs to be conducted to determine whether UV emission from the Gd^{3+} ion is having a positive pumping effect on blue EL emission. Additionally, the observed blue-shift in going from SrS:Er to SrS:Er,Gd suggests that the addition of Gd to other ACTFEL phosphors may also lead to a blue-shift. Finally, note that the SrS:Er,Gd ACTFEL device blue emission is quite broad (i.e. centered at 470 nm with a half-width extending from approximately 400 to 540 nm). The broad nature of the SrS:Er,Gd emission suggests that it could be useful as one half of a white ACTFEL device if its brightness can be sufficiently increased.

The observed decrease in the crystallization temperature of a CaS:Sm ACTFEL device when NaF is used as a flux is very encouraging. Future work should

explore NaF fluxing with other CaS ACTFEL materials such as CaS:Cu. Additionally, the effect of other alkaline metal fluoride fluxes (e.g. KF and LiF) should be investigated.

Bibliography

[1] J. DeMent, *Flourescent Chemicals and Their Applications.* New York: Chemical Publishing Co. Inc., 1942.

[2] Destriau, "Recherches sur les scintillations des sulfures de zinc aux rayons," *J. de Chimie Physique*, vol. 33, pp. 587–625, 1936.

[3] N. Vlasenko and I. Poplov, "Study of the electroluminescence of a sublimed ZnS-Mn phosphor," *Optics and Spectoscopy*, vol. 8, pp. 39–42, 1960.

[4] M. Russ and O. Kennedy, "The effects of double insulating layers on the electroluminescence of ZnS:Mn films," *J. Electrochem. Soc.*, vol. 114, p. 1066, 1967.

[5] T. Inoguchi, M. Takeda, Y. Kakihara, Y. Nakata, and M. Yoshida, "Stable high luminance thin-film electroluminescent panels," *SID Digest*, p. 84, 1974.

[6] Y. Ono, *Electroluminescent displays.* Singapore: World Scientific, 1995.

[7] P. Alt, "Thin-film electroluminescent displays: device characteristics and performance," *Proc. SID*, vol. 25, no. 2, pp. 123–146, 1984.

[8] D. Smith, "Modeling a.c. thin-film electroluinescent devices," *J. Lumin.*, vol. 23, pp. 209–235, 1981.

[9] P. Keir, *Fabrication and Characterization of ACTFEL devices.* PhD thesis, Oregon State University, 1999.

[10] K. Neyts and P. D. Visschere, "Analytical model for thin-film electroluminescent devices," *J. Appl. Phys.*, vol. 68, pp. 4163–4171, Oct. 1990.

[11] E. Bringuier, "Charge transfer in ZnS-type electroluminescence," *J. Appl. Phys.*, vol. 66, pp. 1314–1325, Aug. 1989.

[12] K. Okibayashi, T. Ogura, K. Terada, T. Taniguchi, T. Yamashita, M. Yoshida, and S. Nakajima, "High brightness multi-color EL display panels with black-matrix filter," *SID Digest*, p. 275, 1991.

[13] I. Khormaei, *High resolution EL displays using active matrix approach.* PhD thesis, Oregon State University, 1995.

[14] Y. Fujita, J. Kumata, M. Nishikawa, T. Tohola, T. Matsuoka, A. Abe, and T. Nitta, "Large-scale AC thin-film electroluminescent display panel," *Proc. SID*, vol. 25, pp. 177–182, 1984.

[15] S. Shionoya and W. Yen, eds., *Phosphor Handbook.* Boca Raton: CRC Press, 1999.

[16] F. Cotton, ed., *Chemical Applications of Group Theory.* New York: John Wiley & Sons, third ed., 1990.

[17] G. Blasse and B. Grabmaier, *luminescent materials.* Berlin: Springer-Verlag, 1994.

[18] R. Shannon, "Revised effective ionic radii and systematic studies of interatomic distances in halides and chalcogenides," *Acta Crystallographica A*, vol. 32, p. 751, 1976.

[19] P. Keir, J. Wager, B. Clark, D. Li, and D. Keszler, "Alkali metal coactivators in SrS:Cu,F thin film electroluminescent devices," *Appl. Phys. Lett.*, vol. 75, no. 10, pp. 1398–1400, 1999.

[20] W. Warren, C. Seager, S. Sun, A. Naman, P. Holloway, K. Jones, and E. Soininen, "Microstructure and atomic effects on the electroluminescent efficiency of SrS:Ce thin film devices," *J. Appl. Phys.*, vol. 82, pp. 5138–5143, Nov. 1997.

[21] A. Hardy, *Handbook of colorimetry.* Cambridge, MA: The Technology Press, 1936.

[22] F. Billmeyer and M. Saltzman, *Principles of color technology.* New York: John Wiley & Sons, second ed., 1981.

[23] R. Overheim and D. Wagner, *Light and Color.* New York: John Wiley & Sons, 1982.

[24] B. Baukol, P. Keir, and J. Wager, "Electroluminescent thermal quenching in SrS:Cu thin-film electroluminescent devices," *Appl. Phys. Lett.*, pp. 185–187, 1999.

[25] S. Sun, "Blue emitting SrS:Ag,Cu TFEL devices," *Extended abstracts of the fourth international conference on the science and technology of display phosphors/ the ninth international workshop on inorganic and organic electroluminescence*, pp. 183–186, Sept. 1998.

[26] W. Park, T. Jones, E. Mohammed, C. Summers, and S. Sun, "Luminescence properties of SrS:Cu,Ag thin-film electroluminescent phosphors," *Extended abstracts of the fourth international conference on the science and technology of display phosphors/ the ninth international workshop on inorganic and organic electroluminescence*, pp. 215–218, Sept. 1998.

[27] W. Park, T. Jones, and C. Summers, "Optical properties of SrS:Cu,Ag two-component phosphors for electroluminescent devices," *Appl. Phys. Lett.*, Mar. 1999.

[28] R. Brook, S. Howlett, and S. Wu, *The use of solid solution additives in sintering*, pp. 2135–2144. Amsterdam: Elsevier Scientific, 1982. D. Kolar, S. Pejornik, and M.M. Ristic eds.

[29] R. German, *Sintering theory and practice.* New York: John Wiley & Sons, 1996.

[30] J. Lewis, K. Waldrip, M. Davidson, D. Moorehead, P. Holloway, and S. Sun, "Improved brightness and efficiency in EL thin-film phosphors by fluxing," *Extended abstracts of the fourth international conference on the science and technology of display phosphors/ the ninth international workshop on inorganic and organic electroluminescence*, pp. 227–230, Sept. 1998.

[31] K. Velthaus, B. Huttl, U. Troppenz, R. Herrman, and R. Mauch, "New deposition process for very blue and bright SrS:Ce,Cl TFEL devices," *SID Digest*, pp. 411–414, 1997.

[32] J. Wager, "Thermodynamics and kinetics of vacancy self-compensation in wide-bandgap semiconductors," *Philos. Mag. A*, vol. 67, no. 4, pp. 897–904, 1993.

[33] J. Wager, *Electroluminescent Phosphors: Point Defects.* Berlin: Wissenschaft und Technik Verlag, 1996. R.H. Mauch and H.E. Gumlich eds.

[34] F. Krogen, *The Chemistry of Imperfect Crystals.* Amsterdam: North-Holland Publishing Co., second ed., 1974.

[35] D. Li, *Phosphor development: synthesis, characterization, and chromatic control.* PhD thesis, Oregon State University, 1999.

[36] S. Wolf and R. Tauber, *Silicon Processing for the VLSI Era Vol.1- Process Technology.* Sunset Beach, CA: Lattice Press, 1986.

[37] B. Chapman, *Glow discharge processes.* New York: John Wiley & Sons, 1980.

[38] T. Suntola and J. Hyvarinen, "Atomic layer epitaxy," *Annu. Rev. Mater. Sci.*, vol. 15, pp. 177–195, 1985.

[39] M. Leppanen, M. Leskela, L. Niinisto, E. Nykanen, P. Soininen, and M. Tiitta, "Blue emitting ACTFEL structure based on cerium-activated strontium sulfide grown by atomic layer epitaxy," *SID Symp.*, p. 282, 1991.

[40] H. Kaufman, J. Cuomo, and J. Harper, "Technology and applications of broad-beam ion sources used in sputtering. part i. ion source technology," *J. Vac. Sci. Technol.*, vol. 21, pp. 725–736, Sept. 1982.

[41] H. Kaufman, "Broad-beam ion sources: Present status and future directions," *J. Vac. Sci. Technol.*, vol. 4, pp. 764–771, May 1986.

[42] J. Harper, J. Cuomo, and H. Kaufman, "Technology and applications of broad-beam ion sources used in sputtering. part ii. applications," *J. Vac. Sci. Technol.*, vol. 21, pp. 737–756, Sept. 1982.

[43] A. Fuh, R. Gallinger, P.Schuster, J. Adolph, and O. Caporaletti, "The effects of post-deposition annealing on ZnS:Mn film crystalline structure and electroluminescent characteristics," *Thin Solid Films*, vol. 10, pp. 202–205, Jan. 1992.

[44] A. Kun, D. Leskell, P. Malmberg, J. Murphy, and L. Sienkiewicz, "The influence of chlorine on the crystal structure and electroluminescnt behaviour of ZnS:Mn film crystalline structure and electroluminescent characteristics," *J. Electron. Mater.*, vol. 10, pp. 287–300, Jan. 1981.

[45] S. Takata, T. Minami, and T. Miyata, "Crystallinity of emitting layer and electroluminescence characteristics in multicolour ZnS thin film electrolumi-

nescent device with a thick dielectric ceramic insulating layer," *Thin Solid Films*, vol. 193-4, pp. 481–488, Dec. 1990.

[46] Y. Nakanishi, Y. Fukuda, Y. Matanaka, and G. Shimaoka, "The dependence of the polycrystalline structure and electroluminescent properties of ZnS:Mn deposited on Y_2O_3 films on thickness," *Appl. Surf. Sci.*, vol. 48-9, pp. 297–300, May 1991.

[47] S. Okamoto, T. Kuki, and T. Suzuki, "SrS:Ce thin-film electroluminescent devices fabricated by post-annealing technique and their electrical properties," *Jpn. J. Appl. Phys.*, vol. 32, no. 4A, pp. 1672–1680, 1993.

[48] C. Sawyer and C. Tower, "Rochelle salt as a dielectric," *Phys. Rev.*, vol. 35, pp. 269–273, 1930.

[49] J. Wager and P. Keir, "Electrical characterization of thin-film electroluminescent devices," *Annu. Rev. Mater. Sci.*, vol. 27, pp. 223–248, 1997.

[50] G. Mueller, "Measuring on thin film electroluminescent devices," *Phys. Stat. Sol. a*, vol. 139, p. 271, 1993.

[51] J. Wager, J. Davidson, and D. Morton, "Electrical characterization and modeling of ACTFEL devices," in *6th international workshop on electroluminescence*, (El Paso, Texas, USA), pp. 92–101, May 1992.

[52] A. Douglas, "Alternating-current thin-film electroluminescent device physics and modeling," Master's thesis, Oregon State University, 1993.

[53] R. McArthur, J. Davidson, J. Wager, I. Khormaei, and C. King, "Capacitance-voltage characteristics of alternating-current thin-film electroluminescent devices," *Appl. Phys. Lett.*, vol. 56, pp. 1889–1891, May 1990.

[54] J. Davidson, J. Wager, I. Khormaei, C. King, and R. Williams, "Electrical characterization and modeling of alternating-current thin-film electroluminescent devices," *IEEE Trans. Electron Devices*, vol. 39, May 1992.

[55] J. Davidson, "Capacitance-voltage analysis, SPICE modeling, and aging studies of AC thin-film electroluminescent devices," Master's thesis, Oregon State University, 1991.

[56] S. Shih, P. Keir, and J. Wager, "Space charge generation in ZnS:Mn alternating current thin-film electroluminescent devices," *J. Appl. Phys.*, vol. 78, pp. 5775–5781, Nov. 1995.

[57] J. Hitt, P. Keir, J. Wager, and S. Sun, "Static space charge in evaporated ZnS:Mn alternating-current thin-film electroluminescent devices," *J. Appl. Phys.*, vol. 83, pp. 1141–1145, Jan. 1998.

[58] A. Abu-Dayah, S. Kobayashi, and J. Wager, "Internal charge-phosphor field characteristics of alternating-current thin-film electroluminescent devices," *Appl. Phys. Lett.*, vol. 62, pp. 744–746, Feb. 1993.

[59] A. Abu-Dayah, "Internal charge-phosphor field analysis, electrical characterization, and aging studies of ac thin-film electroluminescent devices," Master's thesis, Oregon State University, 1993.

[60] A. Kitai, "Thin film electroluminescent oxide phosphors," *Extended abstracts of the fourth international conference on the science and technology of display phosphors/ the ninth international workshop on inorganic and organic electroluminescence*, pp. 199–202, Sept. 1998.

[61] T. Minami, "Oxide phosphor thin film electroluminescent devices using thick insulating ceramic sheets," *Extended abstracts of the fourth international conference on the science and technology of display phosphors/ the ninth international workshop on inorganic and organic electroluminescence*, pp. 195–198, Sept. 1998.

[62] A. Levine and F. Palilla, "A new highly efficient red-emitting cathodoluminescent phosphor ($YVO_4 : Eu$) for color television," *Appl. Phys. Lett.*, vol. 5, no. 6, pp. 118–120, 1964.

[63] M. Royce and A. Smith *Ext. Abst. Electrochem. Soc. Spring Meeting*, vol. 34, p. 94, 1968.

[64] T. Kano, K. Kinameri, and S. Sek, "A red phosphor of high lumen equivalent $Y_2W_3O_{12} : Eu(3+)$," *J. Electrochem. Soc.*, vol. 129, p. 2296, 1982.

[65] Y. Tseng, B. Chion, C. Peng, and L. Ozawa, "Spectral properties of Eu^{2+}-activated yttrium oxysulfide red phosphor," *Thin Solid Films*, vol. 330, pp. 173–177, 1998.

[66] K. Sowa, M. Tanabe, S. Furnkawa, Y. Nakanishi, and Y. Hatanka, "Growth of $Y_2O_2 : Eu$ thin films by reactive magnetron sputtering and electroluminescent characteristics," *Jpn. J. Appl. Phys.*, vol. 32, pp. 5601–5602, 1993.

[67] B. Cleary, "VIQ thin-film electroluminescent device physics and modeling," Master's thesis, Oregon State University, 1999.

[68] Y. J. Cho, T. Hivakawa, K. Sakiyama, H. Okamoto, and Y. Hamakawa, "$ZnF_2 : Gd$ thin film electroluminescent device," *Appl. Surf. Sci.*, vol. 113-4, pp. 705–708, 1997.

[69] N. Yamashita, "Luminescence of the lead dimer center in SrS and SrSe phosphors," *J. Phys. Soc. Jpn.*, vol. 53, pp. 2400–2406, 1984.

[70] S. Asano, N. Yamashita, and Y. Nakao, "Luminescene of the Pb^{2+} ion dimer center in CaS and CaSe phosphors," *Phys. Stat. Sol. b*, vol. 89, pp. 663–673, 1978.

[71] E. Nykanen, S. Lehto, M. Leskela, L. Niinisto, and P. Soininen, "Blue electroluminescence in Pb^{2+} doped CaS and SrS thin films," in *6th international workshop on electroluminescence*, (El Paso, Texas, USA), pp. 199–204, May 1992.

[72] D. Poelman, R. V. Meirhaeghe, B. Vermeersch, and F. Cardon, "Possibilities and limitations of blue electroluminescence in $CaS : Pb^{2+}$ thin films," *J. Phys. D: Applied Phys.*, vol. 30, pp. 465–467, 1997.

[73] S.-H. K. Park, S. J. Yun, Y. S. Kim, J.-S. Kang, K.-I. Cho, and D.-S. Ma, "High-luminance blue-emitting CaS:Pb electroluminescent devices grown using atomic layer deposition," *SID Symp.*, May 2000.

[74] T. Oberacker, G. Schlotterbeck, G. Bilger, D. Braunger, and H. Schock, "Field quenching effect in polycrystalline SrS:Pb and SrS:Ce,Pb thin films for electroluminescent devices," *J. Appl. Phys.*, vol. 60, no. 6, pp. 3526–3531, 1996.

[75] J. Flahaut, *Handbook on the Physics and Chemistry of Rare Earths Vol.4 Non-metallic compounds II*, vol. 4. Amsterdam: North Holland Publishing Co., 1979. K.A. Gschneidner and L. Eyring eds.

[76] S. Tanaka, "Thin-film electroluminescent devices using CaS and SrS," *J. Crystal Growth*, vol. 101, pp. 958–966, 1990.

[77] S. Tanaka, H. Yoshiyama, Y. Mikami, J. Nishiura, S. Ohshio, and H. Kobayashi, "Excitation mechanism in red CaS:Eu and blue SrS:Ce,K TFEL devices," *Proc. Soc. Info. Disp.*, vol. 29, no. 1, pp. 77–81, 1988.

[78] D. Poelman, R. Vercaemst, R. Meirhaeghe, W. Laflere, and F. Cardon, "Influence of growth conditions on the properties of CaS:Eu electroluminescent thin films," *J. Lumin.*, vol. 75, pp. 175–181, 1997.

[79] M. Ando and Y. Ono, "Role of Eu^{3+} luminescent centers in the electro-optical characteristics of red-emitting CaS:Eu thin film electroluminescent devices with memory," *J. Appl. Phys.*, vol. 68, no. 7, pp. 3578–3583, 1990.

[80] Private communications with Dr. Doug Keszler.

[81] Private communication with Beau Baukol.

[82] P. Keir, C. Maddix, B. Baukol, and J. Wager, "Lanthanide doping in ZnS and SrS thin-film electroluminescent devices," *J. Appl. Phys.*, vol. 86, no. 12, pp. 6810–6815, 1999.

[83] S. Okamoto, E. Nakazawa, and Y. Tsuchiya, "Electroluminescence of rare-earth activated SrS thin-films," *Jap. J. Appl. Phys. Part 1*, vol. 28, p. 406, 1989.

[84] E. Chase, R. Hepplewhite, D. Krupka, and D.Kahng, "Electroluminescence of ZnS lumocen devices containing rare-earth and transition-metal fluorides," *J. Appl. Phys.*, vol. 40, pp. 2512–2519, May 1969.

[85] M. Jayaraj and C. Vallabhan, "AC thin film electroluminescent devices with rare earth doped ZnS," *J. Electrochem. Soc.*, vol. 138, pp. 1512–1516, May 1991.

[86] S. Okamoto and E. Nakazawa, "Transient emission mechanisms in thin-film electroluminescent devices with rare-earth-activated SrS phosphor layers," *Jpn. J. Appl. Phys.*, vol. 34, pp. 521–526, Feb. 1995.

[87] K. Wickerscheim and R. Lefever, "Luminescent behavior of the rare-earths in yttrium oxide and related hosts," *J. Electrochem. Soc.*, vol. 111, pp. 47–51, 1964.

[88] A. D'Silva and V. Fassel, "X-ray excited optical luminescence in yttrium-gadolinium-terbium phosphate system," *J. Lumin.*, vol. 8, pp. 375–382, 1974.

[89] C. Schaffer and C. Jorgensen, "The nephelauxetic series of ligands corresponding to increasing tendency of partly covalent bonding," *J. Inorg. Nucl. Chem.*, vol. 8, pp. 143–148, 1958.

[90] T. O'Brien, P. Rack, P. Holloway, and M. Zerner, "Crystal field and molecular orbital calculations of the optical transitions in Ce doped alkaline earth sulfide (MgS, CaS, SrS, and BaS) phosphors," *J. Lumin.*, vol. 78, pp. 245–257, 1998.